Research Advance to Putzbach et al., eLife. 2017; 6.

CD95L mRNA is toxic to cells

William Putzbach[1,4], Ashley Haluck-Kangas[1,4], Quan Q. Gao[1], Aishe A. Sarshad[3], Elizabeth T. Bartom[2], Austin Stults[1], Abdul S. Qadir[1], Markus Hafner[3] and Marcus E. Peter[1,2,*]

[1] Department of Medicine/Division Hematology/Oncology, Feinberg School of Medicine, and [2] Department of Biochemistry and Molecular Genetics, Northwestern University, Chicago, IL 60611, USA; [3] Laboratory of Muscle Stem Cells and Gene Regulation, NIAMS, NIH, Bethesda, MD 20892, USA.

*Corresponding author: Marcus Peter, E-mail: m-peter@northwestern.edu, phone: 312-503-1291; FAX: 312-503-0189.

[4] Shared first authorship

Keywords:
RNAi, Fas, cancer, CRISPR, cell death, DISE

Abstract

CD95/Fas ligand binds to the death receptor CD95/Fas to induce apoptosis in sensitive cells. We previously reported the CD95L mRNA is enriched in sequences that, when converted to si/shRNAs, are toxic to cells (Putzbach et al., 2017). These si/shRNAs kill all cancer cells through a RNAi off-target effect by targeting critical survival genes. We now report expression of full-length CD95L mRNA, itself, is highly toxic to cells and induces a similar form of cell death. We demonstrate that small RNAs derived from CD95L are loaded into the RNA induced silencing complex (RISC) and that the RISC is required for the toxicity. Drosha and Dicer knock-out cells are highly sensitive to this toxicity, suggesting that processing of CD95L mRNA into small toxic RNAs is independent of both Dicer and Drosha. The data provide evidence that a higher vertebrate transgene can be processed to RNAi-active small RNAs that elicit cellular responses.

Introduction

Activation of CD95/Fas through interaction with its cognate ligand CD95L or receptor-activating antibodies induces apoptosis in sensitive cells (Suda, Takahashi, Golstein, & Nagata, 1993). Virtually all research on CD95 and CD95L has focused on the physical interaction between the two proteins and the subsequent protein-based signaling cascades (Algeciras-Schimnich et al., 2002; Fu et al., 2016; Nisihara et al., 2001; Schneider et al., 1997). However, we have recently shown that the mRNA of CD95 and CD95L harbor sequences that when converted into small interfering (si) or short hairpin (sh)RNAs, cause massive and robust toxicity in all tested cancer cells. These CD95/CD95L-derived si/shRNAs target a network of survival genes, resulting in the simultaneous activation of multiple cell death pathways through RNA interference (RNAi) in a process we called DISE (Death Induced by Survival gene Elimination) (Putzbach et al., 2017). We determined that for an si/shRNA to elicit this form of toxicity, only positions 2-7 of the guide strand, the 6mer seed sequence, are required (Putzbach et al., 2017). More recently, a screen of all 4096 6mer seeds revealed that optimal 6mer seed toxicity requires G-rich seeds targeting C-rich regions in the 3'UTRs of survival genes (Gao et al., 2018).

In this report, we show that expression of the CD95L mRNA, itself, is toxic to cells even without prior conversion to siRNAs. This toxicity is independent of the full-length CD95L protein or expression of the CD95 receptor and resembles DISE. The toxicity involves RNAi, and multiple small RNAs generated within cells from the mRNA of CD95L are loaded into the RNA-induced Silencing Complex (RISC), the key mediator of RNAi (Liu et al., 2004).

Results

CD95L mRNA is toxic to cells

By testing every possible shRNA derived from the CD95L open reading frame (ORF) or its 3'UTR, we recently found a high enrichment of toxic si/shRNAs derived from the CD95L ORF (Putzbach et al., 2017). Most recently we determined that the 6mer seed toxicity observed in many si/shRNAs is due to their nucleotide composition, with G-rich seeds being the most toxic (Gao et al., 2018). When reanalyzing the CD95L ORF-derived shRNAs, we found a significant correlation between the toxicity of the most toxic CD95L-derived shRNAs (Putzbach et al., 2017) and the seed toxicity of the same 6mer seed we recently determined in a screen of all 4096 6mer seeds (Gao et al., 2018). This suggests that CD95L-derived shRNAs kill cancer cells mainly through 6mer seed toxicity.

We therefore wondered whether expression of the CD95L ORF mRNA—without pre-processing into artificial siRNAs—would be toxic to cells. Expression of CD95L protein in most cells kills through induction of apoptosis. Consequently, expressing CD95L in HeyA8 cells, which are highly sensitive to CD95 mediated apoptosis, killed cells within a few hours after infection with a lentivirus encoding CD95L (***Figure 1A***, left panel). Interestingly, severe growth reduction was seen without any signs of apoptosis (not shown) when a CD95L mutant, unable to bind CD95, was expressed ($CD95L^{MUT}$ in ***Figure 1A***, left panel). This mutant carries a Y218R point mutation, which prevents the CD95L protein from binding to CD95 (Schneider et al., 1997), and is expressed at a similar level to wild type (wt) CD95L (***Figure 1B***). To prevent the CD95L mRNA from producing full-length CD95L protein, we also introduced a premature stop codon right after the start codon in the $CD95L^{MUT}$ vector ($CD95L^{MUT}$NP). This construct (containing 4 point mutations and confirmed to produce mRNA with no detectable full-length CD95L protein, ***Figure 1B***) was equally active in reducing the growth of HeyA8 cells when compared to the $CD95L^{MUT}$ vector (***Figure 1A***, left panel). This result suggested that the CD95L mRNA could be toxic to HeyA8 cells without the CD95L protein inducing apoptosis. This was confirmed by expressing the three CD95L constructs in the presence of the oligo-caspase inhibitor zVAD-fmk (***Figure 1A***, center panel). With suppressed apoptosis, all three constructs were now equally toxic to HeyA8 cells. Finally, we tested a HeyA8 CD95 k.o. clone confirmed to express no CD95 protein (Putzbach et al., 2017). In these cells, without the addition of zVAD-fmk, wt CD95L and $CD95L^{MUT}$NP were again equally active in severely reducing the growth of the cells (***Figure 1A***, right panel). Together, these data suggested it is the CD95L mRNA that killed the cells. Cell death was confirmed by quantifying nuclear fragmentation (***Figure 1C***). We also detected a significant increase of ROS in cells expressing $CD95L^{MUT}$NP (***Figure 1D***), which is a characteristic feature of DISE (Hadji et al., 2014; Patel & Peter, 2017). To exclude the possibility that truncated CD95 protein or any part of the CD95 mRNA would play a role in this toxicity, we deleted the CD95 gene in MCF-7 cells (***Figure 1 - figure supplement 1A-E***). Overexpression of wild-type CD95L killed clone FA4 cells, which harbor a complete homozygous deletion of the entire CD95 gene, as well as CD95 protein k.o. clone #21 cells that retain some truncated mRNA expression (***Figure 1E***). To further distinguish the activities of the CD95L mRNA from CD95L protein, we generated a CD95L expression construct in which we introduced 308 (out of 846 nucleotides) silent mutations (CD95L SIL) (***Figure 1 - figure supplement 2A***). The activity of this mutant construct to negatively affect cell growth of CD95

k.o. HeyA8 cells was compared to two independently cloned wt CD95L constructs (WT1 and WT2 in ***Figure 1 - figure supplement 2B***). The mutant SIL construct was equally effective in suppressing cell growth and produced about the same amount of CD95L mRNA (***Figure 1 - figure supplement 2C***). However, the SIL construct only produced about 12 % of WT CD95L protein (***Figure 1 - figure supplement 2C***), again supporting the observation that it is the CD95L RNA and not the protein that elicits toxicity.

CD95L mRNA kills cells through DISE.

After infection with CD95L, CD95 k.o. HeyA8 cells exhibited morphological changes strikingly similar to the changes seen in wt HeyA8 cells after introduction of a CD95L-derived shRNA (shL3) (***Figure 2A, Video 1-4***) suggesting the cells died through a similar mechanism. To determine the cause of cell death induced by CD95L mRNA in HeyA8 CD95 k.o. cells molecularly, we performed an RNA-Seq analysis. We found that expression of CD95L caused preferential downregulation of critical survival genes and not of nonsurvival genes in a control set (***Figure 2B***). In addition, cell death induced by CD95L mRNA resulted in a substantial loss of 11 of the 12 histones detected to be downregulated in cells treated with CD95 and CD95L-derived sh/siRNAs (***Figure 2C***). Loss of histons is an early event during DISE (Putzbach et al., 2017). A Metascape analysis demonstrated that nucleosome assembly, regulation of mitosis, and genes consistent with the involvement of histones were among the most significantly downregulated RNAs across all cells in which DISE was induced by any of the four sh/siRNAs or by the expression of CD95L mRNA (***Figure 2D***). This suggests that CD95L mRNA kills cells in the same way as CD95/L-derived si/shRNAs.

CD95L mRNA kills cells through RNAi

Given our previous work on CD95L-derived si/shRNA toxicity, we hypothesized that CD95L mRNA kills cells through an RNAi-based mechanism—perhaps by being processed into small RNAs that incorporate into the RISC. Drosha k.o. cells lacking the majority of endogenous miRNAs, but retaining expression of Ago proteins, were shown to be hypersensitive to DISE induced by si- and shRNAs (Putzbach et al., 2017). We interpreted this effect as being caused by an increased pool of unoccupied RNAi machinery caused by the absence of most miRNAs. Drosha k.o. cells were also hypersensitive to the expression of $CD95L^{MUT}NP$ (***Figure 3A,*** p=0.014, according to a polynomial fitting model); Virtually all cells died (insert in ***Figure 3A***).

To directly determine whether the RISC is involved in the toxicity, we introduced CD95L into CD95 k.o. HeyA8 cells after knocking down AGO2 (***Figure 3B***). Knock down of AGO2 was efficient (insert in ***Figure 3B***). Toxicity elicited by CD95L was severely blunted following AGO2 knockdown, suggesting that AGO2 was required for CD95L mRNA to be toxic.

To test the hypothesis that Drosha k.o. cells were more sensitive because their RISC was not occupied by large amounts of nontoxic miRNAs and to determine whether CD95L mRNA could give rise to small RNAs that incorporate into the RISC, we pulled down AGO1-4-associated RNAs and analyzed their composition in wt and Drosha k.o. cells after expressing the CD95L^{MUT}NP mRNA. For the pull-down, we used a peptide—derived from the AGO-binding partner GW182—recently described to bind to all four Ago proteins (Hauptmann et al., 2015). As expected in wt HCT116 cells, large amounts of small RNAs (19-23nt in length) were detected bound to the Ago proteins (***Figure 3C***). Both AGO1 and AGO2 were efficiently pulled down. In contrast, in the Drosha k.o. cells, which cannot generate canonical miRNAs, only a low amount of small RNAs was detected, confirming the absence of miRNAs in the RISC. Surprisingly, the amount of pulled down Ago proteins was severely reduced despite the fact these Drosha k.o. cells express comparable levels of AGO2 (Putzbach et al., 2017). This suggests the peptide did not have access to the Ago proteins in Drosha k.o. cells, presumably because it only binds to Ago proteins complexed with RNA as recently shown (Elkayam et al., 2017).

The analysis of all Ago-bound RNAs showed that in the wt cells, >98.4% of bound RNAs were miRNAs. In contrast, only 34% of bound RNAs were miRNAs in Drosha k.o. cells (***Figure 3D*** and data not shown). These include miRNAs that are processed independently of Drosha such as miR-320a (Kim, Kim, & Kim, 2016). Consistently, this miRNA became a major RNA species bound to Ago proteins in Drosha k.o. cells (***Figure 3D***). In both wt and Drosha k.o. cells, a significant increase in CD95L-derived small RNAs bound to the Ago proteins was detected compared to cells infected with pLenti empty vector. They corresponded to 0.0006% and 0.043% of all the Ago-bound RNAs in the wt cells and Drosha k.o. cells, respectively. Toxicity of CD95L mRNA was, therefore, not due to overloading the RISC. In the absence of most miRNAs, the total amount of RNAs bound to Ago proteins in the Drosha k.o. cells was roughly 10% of the amount bound to Ago in wt cells (***Figure 3D***). The reduction of Ago-bound miRNAs in Drosha k.o. cells (***Figure 3E***, top row) was paralleled by a substantial increase in binding of other small RNAs to the Ago proteins (***Figure 3E***, bottom row). Interestingly, the amount of Ago-bound CD95L-derived small RNAs was >100 times higher in the Drosha k.o. cells

170 compared to the wt cells (red columns in ***Figure 3E***). These data support our hypothesis that
171 Drosha k.o. cells are more sensitive to CD95L mRNA-mediated toxicity due to their ability to
172 take up more toxic small CD95L-derived RNAs into the RISC in the absence of most miRNAs.
173
174 **CD95L ORF is degraded into small RNA fragments that are then loaded into the RISC.**
175 Interestingly, not only did Ago proteins in Drosha k.o. cells bind much more CD95L-derived
176 small RNAs than in the wt cells, but also the peak length of the most abundant Ago-bound RNA
177 species increased from 20 to 23 nt (***Figure 4A***, top panel). To determine the sites within the
178 CD95L mRNA that gave rise to small Ago-bound RNAs, we aligned all small Ago-bound RNAs
179 detected in all conditions to the CD95L ORF sequence (***Figure 4B and C***). We identified 22
180 regions in the CD95L ORF that gave rise to small RNAs that could be bound by Ago proteins
181 (***Figure 4B***). To determine whether these small RNAs were formed in the cytosol and then
182 loaded into the RISC, we also aligned all small RNAs in the total RNA fraction isolated from
183 $CD95L^{MUT}NP$ expressing HCT116 Drosha k.o. cells with CD95L (***Figure 4C***). Interestingly,
184 very similar regions of small RNAs were found. Moreover, the mean as well as the peak of the
185 distribution of the read lengths of small RNAs bound to Ago proteins was smaller than in the
186 total small RNAs fraction (***Figure 4A***, center panel), suggesting these fragments were trimmed
187 to the appropriate length either right before they are loaded into the RISC or by the RISC itself.
188 This was most obvious for the small RNAs in cluster 3 (***Figure 4B and C***). We also noticed that
189 certain small RNAs were more abundant in the Ago-bound fraction when compared to total RNA
190 relative to all other RNAs. To determine whether this type of processing was specific for
191 HCT116 Drosha k.o. cells, we analyzed the Ago-bound small CD95L-derived RNAs in HeyA8
192 CD95 k.o. cells after expression of wt CD95L (***Figure 4D***) and compared them with the total
193 RNA fraction (***Figure 4E***). While we found fewer CD95L-derived reads in these cells, the
194 general location of some of the read clusters overlapped with the ones found in the Drosha k.o.
195 cells and again both the mean and peak of the distribution of RNA lengths was smaller in the
196 Ago-bound fraction versus the total RNA fraction (***Figure 4A***, bottom panel). Together, these
197 data suggest that CD95L mRNA can be processed into smaller RNA fragments, which are then
198 trimmed to a length appropriate for incorporation into the RISC.
199 Our data suggest that the CD95L mRNA, when overexpressed, is toxic to cells due to the
200 formation of Ago-bound small RNAs that are incorporated into the RISC and kill cells through
201 RNAi. This process is independent of Drosha. To determine whether Dicer is required for either

processing of CD95L mRNA or loading the small RNAs into the RISC, we expressed CD95L^{MUT}NP in wt and Dicer k.o. HCT116 cells (***Figure 4F***). Dicer k.o. cells were still sensitive to toxicity induced by CD95L mRNA expression, suggesting the toxicity of the CD95L mRNA does not require the processing by either Drosha or Dicer. Using custom real-time qPCR primers designed to specifically detect the small RNAs from clusters 8 and 21, we detected, in both wt and Dicer k.o. cells over-expressing CD95L^{MUT}NP, fragments from these clusters (***Figure 4G***), demonstrating that Dicer is not involved in processing CD95L mRNA.

All the reported small RNAs derived from CD95L corresponded to the sense strand of the expressed mRNA, raising the question of how they could be processed into double-stranded siRNAs in the absence of an antisense strand. To get a preliminary answer to this question, we subjected the CD95L ORF mRNA sequence to a secondary structure prediction (***Figure 4 - figure supplement 1A***). According to this analysis, the CD95L ORF mRNA forms a tightly folded structure with many of the small RNAs of the 22 clusters juxtaposing each other in stem-like structures creating regions of significant complementarity. These may provide the duplexes needed to be processed and loaded into the RISC. Interestingly, many of the juxtaposing reads were found in duplex structures with 3' overhangs. Three of these oligonucleotides (derived from clusters 7, 15 and 22) when expressed as siRNAs were toxic to HeyA8, H460, M565 and 3LL cells (***Figure 4 - figure supplement 1B)***.

In summary, our data suggest that si- and/or shRNAs with certain seed sequences as they are present in CD95 and CD95L and the entire CD95L ORF are toxic to cancer cells. The CD95L mRNA is broken down into small RNA-active fragments that are loaded into the RISC and then target critical survival genes. This results in cell death through 6mer seed toxicity. The process is independent of both Drosha and Dicer. Finally, the data suggest that a high miRNA content, by "filling up" the RISC, might render cells less sensitive to this form of cell death.

Discussion

We recently reported a novel form of cell death that was observed after expression of si/shRNAs designed from the sequences of CD95/CD95L mRNA (Putzbach et al., 2017). More recently we described that cells die from a loss of multiple survival genes through a mechanism we call 6mer seed toxicity (Gao et al., 2018). The most toxic si/shRNAs derived from CD95 or CD95L were found in the ORF of CD95L (Putzbach et al., 2017). This pointed toward the CD95L mRNA, itself being toxic.

We now show that expression of full-length CD95L mRNA triggers toxicity that is independent of the protein product and canonical apoptosis. This is intriguing considering previous studies showed transgenic expression of CD95L using viruses killed multiple cancer cells that were completely resistant to CD95 mediated apoptosis after addition of agonist anti-CD95 antibodies (ElOjeimy et al., 2006; Hyer, Voelkel-Johnson, Rubinchik, Dong, & Norris, 2000; Sudarshan et al., 2005; Sun et al., 2012). These results were interpreted as intracellular CD95L triggering apoptosis. However, we now provide an alternate explanation—namely, both the CD95L protein *and* mRNA are toxic to cells through distinct mechanisms. The protein induces apoptosis, and the mRNA induces toxicity through an RNAi-based mechanism.

We demonstrate that Dicer and Drosha are not involved in generating the Ago-bound CD95L-derived fragments but there are several candidate RNases that are capable of processing mRNAs. Given the differences in length distribution between the cytosolic versus Ago-bound RNA fragments, it is likely the released CD95L-derived fragment intermediates are incorporated into the RISC and then trimmed to the appropriate length by Ago. Indeed, a similar mechanism is known to occur during the maturation of the erythropoietic miR-451, where the pre-miRNA is first cleaved by AGO2 and then trimmed at the 3' end to the final mature form by the exoribonuclease PARN (Yoda et al., 2013). Furthermore, a similar process occurs with the recently identified class of Ago-bound RNAs called agotrons (Hansen et al., 2016), which consist of an excised intron loaded into the RISC in a manner independent of Drosha or Dicer pre-processing. After trimmed to the appropriate size, the guide RNAs in complex with the RISC can regulate gene expression through RNAi.

Our data provide the first evidence of an overexpressed cDNA to be toxic via an RNAi-dependent mechanism. It was first shown in plants that overexpressed transgenes can be converted into RNAi active short RNA sequences (Hamilton & Baulcombe, 1999). Our data on the effects of overexpressed CD95L RNA, while mechanistically distinct from what was reported in plants, maybe the first example of transgene determining cell fate through the RNAi mechanism in mammalian cells.

A major question that arises from our data is whether CD95L mRNA is toxic *in vivo*. We and others have noticed upregulation of CD95L in multiple stress-related conditions such as after treatment with chemotherapy ((Friesen, Fulda, & Debatin, 1999) and data not shown). While the amount of CD95L mRNA and the level of upregulation alone may not be enough to be toxic, it could be the combination of multiple RNA fragments, derived from multiple different mRNAs

that are generated to kill cells (Putzbach et al., 2018). We view CD95L as just one of many RNAs that have this activity. Indeed, it is unlikely CD95L is the only gene whose mRNA is toxic to cells, as this mRNA-based level of toxicity would be redundant with the potent killing capacity of the CD95L protein. Also, upregulating an mRNA that, by itself, could decimate the cells that would otherwise need to upregulate that mRNA to carry out their biological function in the first place, such as activated T cells upregulating CD95L to mount an immune response, would be self-defeating. Therefore, nature likely distributed this mRNA-based toxicity-inducing capacity over many genes in the genome to prevent activating it when any one of those genes is upregulated during specific cellular processes. It is more likely there exists an entire network of these genes that can release toxic small RNAs when the appropriate stimulus is encountered. Consistent with this hypothesis we recently identified other genes that contain sequences that when converted to shRNAs kill cancer cells through 6mer seed toxicity (Patel & Peter, 2017). Future work will be aimed at identifying additional genes and the mechanism through which they are processed and under what conditions to kill cells.

281 **Materials and methods**

Key Resources Table

Reagent type (species) or resource	Designation	Source or reference	Identifiers	Additional information
Gene (Homo sapiens)	CD95L	NA	NM_000639	
Gene (H. sapiens)	CD95	NA	NM_000043	
Cell line (H. sapiens)	MCF-7	ATCC	ATCC: HTB-22	Human adenocarcinoma of the mammary gland, breast; derived from metastatic site: pleural effusion
Cell line (H. sapiens)	MCF-7 CD95 ΔshR6 clone #21	this paper	NA	MCF-7 CD95 ΔshR6 clone #21 with homozygous 227 nucleotide deletion of the shR6 target site in CD95 (chr10:89,008,920-89,009,146; Human Dec. 2013 GRCh38/hg38 assembly) produced using CRISPR/Cas9 technology; verified homozygous CD95 protein knockout
Cell line (H. sapiens)	MCF-7 CD95 deletion clone FA4	this paper	NA	MCF-7 CD95 deletion clone FA4 with a homozygous deletion of the entire CD95 gene (chr10:88,990,657 - 89,015,785; Human Dec. 2013 GRCh38/hg38 assembly) produced using CRISPR/Cas9 technology; verified homozygous CD95 protein knockout
Cell line (H. sapiens)	HeyA8	PMID: 4016745	RRID: CVCL_8878	Human high grade ovarian serous adenocarcinoma; derived from parent Hey cells (RRID: CVCL_0297)

Cell line (H. sapiens)	HeyA8 shR6 k.o. clone #11, HeyA8 CD95 k.o.	PMID: 29063830	NA	HeyA8 CD95 k.o. clone with a homozygous 227 nucleotide deletion of the shR6 target site in CD95 (chr10:89,008,920-89,009,146; Human Dec. 2013 GRCh38/hg38 assembly) produced using CRISPR/Cas9 technology; verified homozygous CD95 protein knockout
Cell line (H. sapiens)	HCT116	Korean Collection for Type Cultures (KCTC)	KCTC: cat#HC19023; ATCC: CCL_247	Human colorectal carcinoma
Cell line (H. sapiens)	Drosha$^{-/-}$; Drosha$^{-/-}$ clone #40	Korean Collection for Type Cultures (KCTC); PMID: 26976605	KCTC: cat#HC19020	HCT116 clone #40 with homozygous protein knockout of Drosha; knockout achieved using CRISPR/Cas9 which resulted in a single nucleotide insertion in one allele and a 26 nucleotide deletion in the other
Cell line (H. sapiens)	Dicer$^{-/-}$; Dicer$^{-/-}$ clone #43	Korean Collection for Type Cultures (KCTC); PMID: 26976606	KCTC: cat#HC19023	HCT116 clone #43 with homozygous protein knockout of Dicer; knockout achieved using CRISPR/Cas9 which resulted in a three nucleotide insertion and 14 nucleotide deletion in one allele and a 35 nucleotide deletion in the other
Cell line (H. sapiens)	Dicer$^{-/-}$; Dicer$^{-/-}$ clone #45	Korean Collection for Type Cultures (KCTC); PMID: 26976607	KCTC: cat#HC19024	HCT116 clone #45 with homozygous protein knockout of Dicer; knockout achieved using CRISPR/Cas9 which resulted in a 53 nucleotide deletion in one allele and a 28 nucleotide deletion in the other
Cell line (H. sapiens)	293T	ATCC	ATCC: CRL-3216	Derived from HEK293 cells (ATCC: CRL-1573); express large T antigen; used for packaging viruses
Cell line (H. sapiens)	H460	ATCC	ATCC: #HTB-177	Human lung pleural effusion carcinoma
Cell line (Mus musculus)	3LL	ATCC	ATCC #CRL-1642	Mouse Lewis lung carcinoma

Cell line (Mus musculus)	M565	PMID: 25366259	NA	Mouse hepatocellular carcinoma isolated from naturally occurring tumor in a floxed CD95 background
Antibody	anti-human AGO1 (rabbit monoclonal)	Cell Signaling	Cell Signaling #5053	1:2000; for western blot; primary Ab
Antibody	anti-human AGO1 (rabbit polyclonal)	Abcam	Abcam #98056	1:2000; for western blot; primary Ab
Antibody	anti-human AGO2 (rabbit polyclonal)	Abcam	Abcam #32381	1:2000; for western blot; primary Ab
Antibody	Goat anti-rabbit, IgG-HRP	Southern Biotech	Southern Biotech: cat#SB-4030-05	1:5000; for western blot; secondary Ab
Antibody	Goat anti-rabbit, IgG-HRP	Cell Signaling	Cell Signaling: cat#7074	1:2000; for western blot; secondary Ab
Antibody	Goat anti-mouse; IgG1-HRP	Southern Biotech	Southern BioTech: cat#1070-05	1:5000; for western blot; secondary Ab
Recombinant protein reagent	LzCD95L	PMID: 14504390	NA	Leucine zipper tagged CD95L; recombinant protein
Chemical compound	CellTiter-Glo	Promega	Promega #G7570	Detects ATP release as a surrogate for cell death; read-out is fluorescence
Chemical compound	propidium iodide	Sigma-Aldrich	Sigma-Aldrich: cat#P4864	Used for subG1 flow cytometry analysis
Chemical compound	puromycin	Sigma-Aldrich	Sigma-Aldrich: cat#P9620	Used for selection of cells expressing puromycin resistance cassettes
Chemical compound	G418	Affymetrix	Affymetrix: cat#11379	Used for selection of cells expressing G418 resistance cassette
Chemical compound	2',7'-dichlorodihydrofluorescein diacetate	Thermofisher Scientific	Thermofisher Scientific #D399	Dye used for detecting ROS production

Chemical compound	zVAD-fmk	Sigma-Aldrich	Sigma-Aldrich: cat#V116	Used at 20uM; pan caspase inhibitor
Recombinant DNA reagent	pLenti-GIII-CMV-RFP-2A-Puro vector; pLenti	ABM Inc	NA	pLenti control empty lentiviral vector; carries an RFP-2a-puromycin resistance cassette
Recombinant DNA reagent	pLenti-CD95L	this paper	NA	pLenti-GIII-CMV-RFP-2A-Puro vector that expresses human wild type CD95L cDNA (NM_000639.2); used to express wt human CD95L upon infection with lentiviral particles
Recombinant DNA reagent	pLenti-CD95L^{MUT}	this paper	NA	pLenti-GIII-CMV-RFP-2A-Puro vector that expresses human CD95L cDNA (NM_000639.2) with 2 nucleotide substitutions in codon 218 (TAT -> CGT) resulting in replacement of tyrosine for arginine (Y218R mutation); unable to bind CD95
Recombinant DNA reagent	pLenti-CD95L^{MUT}NP	this paper	NA	pLenti-GIII-CMV-RFP-2A-Puro vector that expresses human CD95L cDNA (NM_000639.2) with both the Y218R mutation and a single nucleotide substitution at the second codon (CAG -> TAG), resulting in a premature stop codon right after the start codon
Recombinant DNA reagent	pLenti-CD95L^{SIL}	this paper	NA	pLenti-GIII-CMV-RFP-2A-Puro vector that expresses human CD95L cDNA (NM_000639.2) with all codons containing synonymous mutations except for select codons in the proline-rich domain to meet IDT synthesis criteria

Transfected construct	gRNA scaffold	PMID: 23287722	IDT: synthesized as gene block	455 nucleotide CRISPR/Cas9 gRNA scaffold synthesized as a gene block; contains promoter, gRNA scaffold, target sequence, and termination sequence; scaffold transcribes gRNAs that target Cas9 endonuclease to cut at target sites; target sequences consist of 19 nucleotides that are complementary to the target site of choice; co-transfected with Cas9 to catalyze cleavage.
Transfected construct	pMJ920 Cas9 plasmid	Addgene; PMID: 23386978	Addgene: cat#42234	Plasmid that expresses a human codon-optimized Cas9 tagged with GFP and HA; used to express Cas9 for CRISPR-mediated deletions.
Chemical compound	Lipofectamine 2000	ThermoFisher Scientific	ThermoFisher Scientific: cat#11668019	Transfection reagent
Chemical compound	Lipofectamine RNAiMAX	ThermoFisher Scientific	ThermoFisher Scientific: cat#13778150	Transfection reagent; used for transfection of small RNAs such as siRNAs
Commercial assay or kit	StrataClone Blunt PCR Cloning Kit	Agilent Technologies	Agilent Technologies: cat#240207	Used to blunt-end clone the gRNA scaffolds into the pSC-B plasmid
Genetic reagent	Taqman Gene expression master mix	ThermoFisher Scientific	#4369016	
Sequence-based reagent	shR6 flanking Fr primer	IDT	IDT: custom DNA oligo	Fr primer that flanks shR6 site; used to detect 227 nt shR6 deletion; 5'-GGTGTCATGCTGTGACTGTTG-3'
Sequence-based reagent	shR6 flanking Rev primer	IDT	IDT: custom DNA oligo	Rev primer that flanks shR6 site; used to detect 227 nt shR6 deletion; 5'-TTTAGCTTAAGTGGCCAGCAA-3'

Sequence-based reagent	shR6 internal Rev primer	IDT	IDT: custom DNA oligo	Rev primer that overlaps with the shR6 site; used to detect 227 nt shR6 deletion; 5'-AAGTTGGTTTACATCTGCAC-3'
Sequence-based reagent	CD95 flanking Fr primer	IDT	IDT: custom DNA oligo	Fr primer that flanks the CD95 gene; used to detect CD95 gene deletion; 5'-TGTTTAATATAGCTGGGGCTATGC-3'
Sequence-based reagent	CD95 flanking Rev primer	IDT	IDT: custom DNA oligo	Rev primer that flanks the CD95 gene; used to detect CD95 gene deletion; 5'-TGGGACTCATGGGTTAAATAGAAT-3'
Sequence-based reagent	CD95 internal Rev primer	IDT	IDT: custom DNA oligo	Rev internal primer that targets within the CD95 gene; used to detect CD95 gene deletion; 5'-GACCAGTCTTCTCATTTCAGAGGT-3'
Sequence-based reagent	siScr	IDT; Dharmacon	Dharmacon #D-001810-02-05	control non-targeting siRNA; sense: UGGUUUACAUGUUGUGUGA
Sequence-based reagent	c7/1	IDT	custom siRNA; antisense strand corresponds to cluster 7 CD95L sequence	antisense: 5'-AUUGGGCCUGGGGAUGUUU-3'; antisense strand designed with 3' deoxy AA; complementary sense strand has 3' deoxy TT and 2'-O-methylation at the first two positions
Sequence-based reagent	c7/2	IDT	custom siRNA; antisense strand corresponds to cluster 7 CD95L sequence	antisense: 5'-CCUGGGGAUGUUUCAGCUC-3'; antisense strand designed with 3' deoxy AA; complementary sense strand has 3' deoxy TT and 2'-O-methylation at the first two positions

Sequence-based reagent	c11	IDT	custom siRNA; antisense strand corresponds to cluster 11 CD95L sequence	antisense: 5'-CCAACUCAAGGUCCAUGCC-3'; antisense strand designed with 3' deoxy AA; complementary sense strand has 3' deoxy TT and 2'-O-methylation at the first two positions
Sequence-based reagent	c15/1	IDT	custom siRNA; antisense strand corresponds to cluster 15 CD95L sequence	antisense: 5'-AAACUGGGCUGUACUUUGU-3'; antisense strand designed with 3' deoxy AA; complementary sense strand has 3' deoxy TT and 2'-O-methylation at the first two positions
Sequence-based reagent	c15/2	IDT	custom siRNA; antisense strand corresponds to cluster 15 CD95L sequence	antisense: 5'-AACUGGGCUGUACUUUGUA-3'; antisense strand designed with 3' deoxy AA; complementary sense strand has 3' deoxy TT and 2'-O-methylation at the first two positions
Sequence-based reagent	c16/1	IDT	custom siRNA; antisense strand corresponds to cluster 16 CD95L sequence	antisense: 5'-CAACAACCUGCCCCUGAGC-3'; antisense strand designed with 3' deoxy AA; complementary sense strand has 3' deoxy TT and 2'-O-methylation at the first two positions
Sequence-based reagent	c16/2	IDT	custom siRNA; antisense strand corresponds to cluster 16 CD95L sequence	antisense: 5'-AACUCUAAGCGUCCCCAGG-3'; antisense strand designed with 3' deoxy AA; complementary sense strand has 3' deoxy TT and 2'-O-methylation at the first two positions

Sequence-based reagent	c21	IDT	custom siRNA; antisense strand corresponds to cluster 21 CD95L sequence	antisense: 5'-UCAACGUAUCUGAGCUCUC-3'; antisense strand designed with 3' deoxy AA; complementary sense strand has 3' deoxy TT and 2'-O-methylation at the first two positions
Sequence-based reagent	c22	IDT	custom siRNA; antisense strand corresponds to cluster 22 CD95L sequence	antisense: 5'-AAUCUCAGACGUUUUUCGG-3'; antisense strand designed with 3' deoxy AA; complementary sense strand has 3' deoxy TT and 2'-O-methylation at the first two positions
Sequence-based reagent	siScr pool	Dharmacon	D-001810-10	control non-targeting siRNA pool
Sequence-based reagent	SMARTpool siRNA targeting AGO2	Dharmacon	L-004639-00-0005	siRNA pool designed to target AGO2
Sequence based reagent (human)	GAPDH primer	Thermofisher Scientific	Hs00266705_g1	RT-qPCR; control probe
Sequence based reagent (human)	CD95L primers	Thermofisher Scientific	Hs00181226_g1; Hs00181225_m1	RT-qPCR
Sequence based reagent (human)	CD95 primers	Thermofisher Scientific	Hs00531110_m1; Hs00236330_m1	RT-qPCR
Sequence based reagent (human)	$CD95L^{SIL}$ primer	Thermofisher Scientific	assay ID: APNKTUD	Custom RT-qPCR primer designed using the Thermofisher Scientific design tool to detect $CD95L^{SIL}$ mRNA

Sequence based reagent (human)	Cluster 8 CD95L small RNA primer	Thermofisher Scientific	custom probe	Custom RT-qPCR primer designed using the Thermofisher Scientific design tool at https://www.thermofisher.com/order/custom- genomic-products/tools/small-rna to specifically detect small RNAs from cluster 8 of CD95L (5'-AAGGAGCTGGCAGAACTCCGAGA-3')
Sequence based reagent (human)	Cluster 21 CD95L small RNA primer	Thermofisher Scientific	custom probe	Custom RT-qPCR primer designed using the Thermofisher Scientific design tool at https://www.thermofisher.com/order/custom- genomic-products/tools/small-rna to specifically detect small RNAs from cluster 21 of CD95L (5'-TCAACGTATCTGAGCTCTCTC-3')
Sequence based reagent (human)	z30 primer	Thermofisher Scientific	ThermoFisher Scientific #4427975	RT-qPCR for small RNA; control probe
Peptide, recombinant protein	Flag-GST-T6B peptide	PMID: 26351695	NA	Peptide derived from GW182 used to pull down AGO1 to 4
Commercial assay or kit	anti-Flag M2 magnetic beads	Sigma-Aldrich	Sigma-Aldrich #M8823	

Reagents and antibodies

All reagents and antibodies were described previously (Putzbach et al., 2017) except those referenced in the following paragraphs.

Cell lines

HeyA8 (RRID:CVCL_8878) and HeyA8 CD95 knock-out cells, HCT116 (ATCC #CCL-247; RRID:CVCL_0291) and HCT116 Drosha knock-out and Dicer knock-out cells, MCF-7 cells (ATCC #HTB-22; RRID:CVCL_0031), and 293T (ATCC #CRL-3216; RRID:CVCL_0063) cells were cultured as described previously (Putzbach et al., 2017). The MCF-7 CD95 knock-out

292 and deletion cells were cultured in RPMI 1640 medium (Cellgro #10-040-CM), 10% heat-
293 inactivated FBS (Sigma-Aldrich), 1% L-glutamine (Mediatech Inc), and 1%
294 penicillin/streptomycin (Mediatech Inc). H460 (ATCC #HTB-177; RRID:CVCL_0459) cells
295 were cultured in RPMI1640 medium (Cellgro Cat#10-040) supplemented with 10% FBS (Sigma
296 Cat#14009C) and 1% L-Glutamine (Corning Cat#25-005). 3LL cells (ATCC #CRL-1642;
297 RRID:CVCL_4358) were cultured in DMEM medium (Gibco Cat#12430054) supplemented
298 with 10% FBS and 1% L-Glutamine. Mouse hepatocellular carcinoma cells M565 cells were
299 described previously (Ceppi et al., 2014) and cultured in DMEM/F12 (Gibco Cat#11330)
300 supplemented with 10% FBS, 1% L-Glutamine and ITS (Corning #25-800-CR). All cell lines
301 were authenticated using STR profiling and tested monthly for mycoplasm using PlasmoTest
302 (Invitrogen).
303
304 **Plasmids and constructs**
305 The pLenti-CD95L was synthesized by sub-cloning an insert containing the CD95L ORF
306 (NM_000639.2; synthesized by IDT as minigene with flanking 5' NheI RE site and 3' XhoI RE
307 sites in pIDTblue vector) into the pLenti-GIII-CMV-RFP-2A-Puro vector (ABM Inc). The insert
308 and the backbone were digested with NheI (NEB #R0131) and XhoI (NEB #R0146) restriction
309 enzymes. Subsequent ligation with T4 DNA ligase created the pLenti-CD95L vector. The
310 pLenti-CD95L^{MUT} vector was created by sub-cloning a CD95L cDNA insert with 2 nucleotide
311 substitutions in codon 218 (*TAT -> CGT)* resulting in replacement of tyrosine for arginine, which
312 has been described to inhibit binding to CD95 (Schneider et al., 1997) into the pLenti-GIII-
313 CMV-RFP-2A-Puro vector. The pLenti-CD95L^{MUT}NP vector was created by inserting a CD95L
314 ORF cDNA sequence containing both the Y218R mutation and a single nucleotide substitution at
315 the second codon (*CAG -> TAG*), resulting in a premature stop codon right after the start codon,
316 into the pLenti-GIII-CMV-RFP-2A-Puro vector. The pLenti-CD95L^{SIL} was created by sub-
317 cloning a mutant CD95L ORF cDNA sequence with codons synonymously mutated (***Figure 1 -***
318 ***figure supplement 2A***) to the next most highly utilized codon in human cells (exceptions were
319 made within the proline rich domain to meet gene synthesis design criteria.) into the pLenti-GIII-
320 CMV-RFP-2A-Puro vector.
321
322 **Overexpression of CD95L cDNAs**

323 All lentiviral constructs were generated in 293T cells as described previously (Putzbach et al.,
324 2017). HeyA8 and MCF-7 (and all derivative cell lines) cells overexpressing wild type CD95L
325 and mutant CD95L cDNAs were generated by seeding cells at 100,000 cells per well in a 6-well
326 plate and infecting cells with lentivirus generated in 293T cells (500 µl viral supernatant per
327 well) with 8 µg/ml Polybrene. Media was changed next day. Selection was started either during
328 the evening of the same day or on following day with 3 µg/ml puromycin. HCT116, HCT116
329 Drosha knockout, and HCT116 Dicer knockout cells (Kim et al., 2016) overexpressing CD95L
330 cDNAs were generated by seeding cells at 100,000 cells per well in a 24-well plate or 500,000
331 cells per well in a 6-well plate and infecting cells with lentivirus generated in 293T cells (100 µl
332 virus per 24-well or 500 µl per 6-well) in the presence of 8 µg/ml Polybrene. Media was changed
333 the next day, and cells were selected with 3 µg/ml puromycin the following day. Infection with
334 empty pLenti was always included as a control.

335 To assess toxicity of overexpressing CD95L cDNAs, cells infected with these constructs
336 were plated in on a 96-well plate 1 day after selection in the presence of puromycin (uninfected
337 cells were all dead after 1 day in presence of puromycin); Cell confluency was assessed over
338 time using the IncuCyte as described previously (Putzbach et al., 2017).

339 To assess overexpression of CD95L cDNAs in apoptosis-sensitive HeyA8 cells in ***Figure***
340 ***1A***, infection with CD95L lentiviruses were done in 96-well plate using 50 µl of virus in the
341 presence of 20 µM zVAD-fmk (Sigma-Aldrich #V116) and 8 µg/ml Polybrene; media was
342 changed next day in the presence of 20 µM zVAD-fmk; 3 µg/ml puromycin was added the
343 following day. Infection with the CD95L constructs for the RT-qPCR and Western blot in
344 ***Figure 1B*** were done in a 6-well plate in the presence of 20 µM zVAD-fmk.

345 For the experiment in ***Figure 3B***, HeyA8 CD95 knock-out cells were reverse transfected
346 in a 6-well plate; 100,000 cells were plated in wells with either the On-TargetPlus non-targeting
347 siRNA (Dharmacon #D-001810-10) or siAGO2 pool (Dharmacon ##L-004639-00-0005) at 25
348 nM complexed with 1 µl RNAiMax. After ~24 hrs, the cells were infected with either pLenti or
349 pLenti-CD95L (500 µl of viral supernatant [25% of total volume]). Next day, media was
350 replaced, and cells were expanded to 10 cm plates. The following day, 3 µg/ml puromycin
351 was added. When puromycin selection was complete (one day later), the 750-1,500 cells were
352 plated per well in a 96-well plate and put in the IncuCyte machine to assess cell confluency over
353 time.
354

355 **CRISPR deletions**

356 We co-transfected a Cas9-expressing plasmid (Jinek et al., 2013) and two gRNAs that target
357 upstream and downstream to delete an entire section of DNA as described previously (Putzbach
358 et al., 2017). The gRNA scaffold was used as described (Mali et al., 2013). The gRNAs were
359 designed using the algorithm found at http://crispr.mit.edu; only gRNAs with a score above 50
360 were considered.

361 A deletion of 227 nucleotides in exon 4 of CD95 in MCF-7 cells (ΔshR6, clone #21) was
362 generated using gRNAs described previously (Putzbach et al., 2017). Deletion of this site results
363 in a frame-shift mutation that causes a protein-level knock-out (Putzbach et al., 2017). PCR with
364 flanking external primers (Fr: 5'-*GGTGTCATGCTGTGACTGTTG*-3' and Rev: 5'-
365 *TTTAGCTTAAGTGGCCAGCAA*-3') and internal primers (Fr primer and the internal Rev primer
366 5'-*AAGTTGGTTTACATCTGCAC*-3') was used to screen for single cell clones that harbor a
367 homozygous deletion.

368 The two sequences targeted by the flanking gRNAs for the deletion of the entire CD95 gene
369 were 5'-GTCAGGGTTCGTTGCACAAA-3' and 5'-TGCTTCTTGGATCCCTTAGA-3'. For
370 detection of the CD95 gene deletion, the flanking external primers were 5'-
371 *TGTTTAATATAGCTGGGGCTATGC*-3' (Fr primer) and 5'-
372 *TGGGACTCATGGGTTAAATAGAAT*-3' (Rev primer), and the internal reverse primer was 5'-
373 *GACCAGTCTTCTCATTTCAGAGGT*-3'. After screening the clones, Sanger sequencing was
374 performed to confirm the proper deletion had occurred.

375

376 **Real-Time quantitative PCR**

377 The relative expression of specific mRNAs was quantified as described previously (Gao et al.,
378 2018). The primer/probes purchased from ThermoFisher Scientific were GAPDH
379 (Hs00266705_g1), human CD95L (Hs00181226_g1 and Hs00181225_m1), human CD95
380 (Hs00531110_m1 and Hs00236330_m1), and a custom primer/probe to detect the $CD95L^{SIL}$
381 mRNA (designed using the Thermofisher Scientific custom design tool; assay ID: APNKTUD).

382 Custom RT-qPCR probes designed to specifically detect small RNA species were used to
383 detect CD95L fragments in ***Figure 4G***. These probes were designed using ThermoFisher's
384 Custom TaqMan Small RNA Assay Design Tool (https://www.thermofisher.com/order/custom-
385 genomic-products/tools/small-rna/) to target the cluster 8 sequence (5'-
386 AAGGAGCTGGCAGAACTCCGAGA-3') and the cluster 21 sequence (5'-

387 TCAACGTATCTGAGCTCTCTC-3'). Detection of these fragments involves a two-step
388 amplification protocol used to detect microRNAs. In the first step, the High-Capacity cDNA
389 reverse transcription kit is used to selectively reverse transcribe the two clusters to be quantified
390 using specific primers and 20 nM RNA input following the manufacturer's protocol. The cDNA
391 is diluted 1:5. The qPCR reaction mixture is composed of the diluted cDNA, the custom probes,
392 and the Taqman Universal PCR Master Mix (Applied Biosystems #43240018). Reactions were
393 performed in triplicate. Ct values were determined using the Applied Biosystems 7500 Real
394 Time PCR system with a thermocycle profile of 50°C for two min (step one), 95°C for 10 min
395 (step two), and then 40 cycles of 95°C for 15 s (step three) and 60°C for 1 min (step four). The
396 ΔΔCt values between the small RNA of interest and the control were calculated to determine
397 relative abundance of the small RNA. Samples were normalized to Z30 (ThermoFisher Scientific
398 #4427975).
399
400 **Western blot analysis**
401 Detection of human CD95, CD95L and Ago proteins was done via Western blot as described
402 previously (Putzbach et al., 2017).
403
404 **CD95 surface staining**
405 Flow cytometry was used to quantify the level of membrane-localized CD95 as described
406 previously (Putzbach et al., 2017).
407
408 **Cell death quantification (DNA fragmentation) and ROS production**
409 The percent of subG1 nuclei (fragmented DNA) was determined by PI staining/flow cytometry
410 as described previously (Putzbach et al., 2017). ROS production was quantified using the cell-
411 permeable indicator 2',7'-dichlorodihydrofluorescein diacetate (ThermoFisher Scientific #D399)
412 as previously described (Hadji et al., 2014).
413
414 **Assessing cell growth and fluorescence over time**
415 After treatment/infection, cells were seeded in a 96-well plate at least in triplicate. Images were
416 captured at indicated time points using an IncuCyte ZOOM live cell imaging system (Essen
417 BioScience) with a 10x objective lens. Percent confluence and total fluorescent integrated
418 intensity was calculated using the IncuCyte ZOOM software (version 2015A).

419

420 **Infection of cells for Ago-pull down and small RNA-Seq analysis**

421 HeyA8 ΔshR6 clone #11 cells were seeded at 75,000 cells per well on 6-well plates, and the
422 HCT116 and HCT116 Drosha knock-out cells were both seeded at 500,000 per well on 6-well
423 plates. The HeyA8 ΔshR6 clone #11 cells were infected with 0.5 mL of empty pLenti or pLenti-
424 CD95L-WT viral supernatant per well. The HCT116 and HCT116 Drosha knockout cells were
425 infected with 0.5 mL empty pLenti or pLenti-CD95L^{MUT}NP viral supernatant per well. Media
426 was changed the next day and the cells were pooled and expanded to multiple 15 cm dishes.
427 Selection with 3 µg/mL puromycin began the following day. The next day, the HeyA8 ΔshR6
428 clone #11 infected cells were seeded at 600,000 cells per dish in multiple 15 cm dishes; the
429 HCT116 and HCT116 Drosha knock-out cells were seeded at 5 million cells per dish in multiple
430 15 cm dishes. Two days later, each of the samples was pelleted and split in two: one pellet was
431 lysed and processed for small RNA sequencing, and the other pellet was flash frozen in liquid
432 nitrogen. The pellets were stored at -80°C until they could be used for the Ago pull-down
433 experiment. The purpose of splitting the sample was so that we could compare the total cellular
434 pool of small RNAs to the fraction that was bound to the RISC. This way, the processing
435 CD95L-derived fragments from the full-length mRNA in the cytosol to the final mature RISC-
436 bound form could be mapped. This was all done in duplicate.

437

438 **RNA-Seq analysis**

439 Total RNA was isolated using the miRNeasy Mini Kit (Qiagen, #74004) following the
440 manufacturer's instructions. An on-column digestion step using the RNase-free DNase Set
441 (Qiagen #79254) was included. Both small and large mRNA libraries were generated and
442 sequenced as described previously (Putzbach et al., 2017). Reads were trimmed with TrimGalore
443 and then aligned to the hg38 assembly of the human genome with Tophat. Raw read counts were
444 assigned to genes using HTSeq and differential gene expression was analyzed with the R
445 Bioconductor EdgeR package (Robinson, McCarthy, & Smyth, 2010).

446

447 **Ago pull down and RNA-Seq analysis of bound small RNAs**

448 Cell pellets were harvest at 50 hours after plating (122 hours after infection) and were flash
449 frozen in liquid nitrogen. The pellets were stored at -80°C until ready for further processing.
450 Between 10 and 25 x 10^6 cells were lysed in NP40 lysis buffer (20 mM Tris, pH 7.5, 150 mM

451 NaCl, 2 mM EDTA, 1% (v/v) NP40, supplemented with phosphatase inhibitors) on ice for 15
452 minutes. The lysate was sonicated 3 times for 30 s at 60% amplitude (Sonics, VCX130) and
453 cleared by centrifugation at 12,000*g* for 20 minutes. AGO1-4 were pulled down by using 500 μg
454 of Flag-GST-T6B peptide (Hauptmann et al., 2015) and with 60 μl anti-Flag M2 magnetic beads
455 (Sigma-Aldrich) for 2 hrs at 4°C. The pull-down was washed 3 times in NP40 lysis buffer.
456 During the last wash, 10% of beads were removed and incubated at 95°C for 5 minutes in 2x
457 SDS-PAGE sample buffer. Samples were run on a 4-12% SDS-PAGE and transferred to
458 nitrocellulose membrane. The pull-down efficiency was determined by immunoblotting against
459 AGO1 (Cell Signaling #5053; RRID:AB_10695871 and Abcam #98056; RRID:AB_10680548)
460 and AGO2 (Abcam #32381; RRID:AB_867543). To the remaining beads 500 μl TRIzol reagent
461 were added and the RNA extracted according to the manufacturer's instructions. The RNA pellet
462 was diluted in 20 μl of water. The sample was split, and half of the sample was dephosphorylated
463 with 0.5 U/μl of CIP alkaline phosphatase at 37°C for 15 min and subsequently radiolabeled with
464 0.5 μCi γ-^{32}P-ATP and 1 U/μl of T4 PNK kinase for 20 min at 37°C. The AGO1-4 interacting
465 RNAs were visualized on a 15% urea-PAGE. The remaining RNA was taken through a small
466 RNA library preparation as previously described (Hafner et al., 2012). Briefly, RNA was ligated
467 with 3' adenylated adapters and separated on a 15% denaturing urea-PAGE. The RNA
468 corresponding to insert size of 19-35 nt was eluted from the gel, ethanol precipitated followed by
469 5' adapter ligation. The samples were separated on a 12% Urea-PAGE and extracted from the
470 gel. Reverse transcription was performed using Superscript III reverse transcriptase and the
471 cDNA amplified by PCR. The cDNA was sequenced on Illumina HiSeq 3000. Adapter
472 sequences: Adapter 1 – NNTGACTGTGGAATTCTCGGGTGCCAAGG; Adapter 2 –
473 NNACACTCTGGAATTCTCGGGTGCCAAGG, Adapter 3 –
474 NNACAGAGTGGAATTCTCGGGTGCCAAGG, Adapter 4 –
475 NNGCGATATGGAATTCTCGGGTGCCAAGG, Adapter 47 –
476 NNTCTGTGTGGAATTCTCGGGTGCCAAGG, Adapter 48 –
477 NNCAGCATTGGAATTCTCGGGTGCCAAGG, Adapter 49 –
478 NNATAGTATGGAATTCTCGGGTGCCAAGG, Adapter 50 –
479 NNTCATAGTGGAATTCTCGGGTGCCAAGG. RT primer sequence:
480 GCCTTGGCACCCGAGAATTCCA; PCR primer sequences:
481 CAAGCAGAAGACGGCATACGAGATCGTGATGTGACTGGAGTTCCTTGGCACCCGAG
482 AATTCCA. To identify CD95L-derived small RNAs among the sequenced reads, a BLAST

483 database was generated from each set of reads, and blastn was used to query the CD95L ORF
484 (derived from NM_000639.2) against reads from cells infected with pLenti-CD95L and to query
485 the CD95L^{MUT}NP ORF sequence against reads from cells infected with CD95L^{MUT}NP. The only
486 reads considered further were those matching a CD95L sequence with an e-value of less than
487 0.05 and 100% identity across the entire length of the read. This resulted in the loss of a few
488 reads less than 19/20 nt in length. The filtered BLAST hits were converted to a bed formatted
489 file, describing the locations of reads relative to the relevant CD95L sequence, and the R
490 package Sushi was used to plot the bed files and generate Figures 4B-E.
491

492 **Assessing toxicity of CD95L-derived small RNAs**

493 To determine whether guide RNAs derived from the over-expressed CD95L mRNA could evoke
494 toxicity, the small CD95L-derived RNA reads (corresponding to different clusters shown in
495 ***Figure 4C***) bound to AGO from the HCT116 Drosha knock-out cells were converted to siRNAs.
496 First, all reads less than 18 nucleotides were filtered out, as these do not efficiently incorporate
497 into the RISC. siRNAs were designed with antisense strands identical to these CD95L-derived
498 sequences that mapped to areas of the CD95L mRNA secondary structure (***Figure 4 - figure***
499 ***supplement 1A***) that are predicted to form duplexes. These sequences were designed as 19
500 nucleotide oligos with a 3' deoxy AA. The complementary sense strand was designed with a 3'
501 deoxy TT and 2'-O-methylation at the first two positions to prevent its incorporation into the
502 RISC. These oligos were ordered from IDT and annealed to form the final siRNAs. The
503 sequences of the antisense strands (corresponding to the CD95L mRNA-derived cluster
504 fragments) were as follows: 5'-AUUGGGCCUGGGGAUGUUU-3' (c7/1), 5'-
505 CCUGGGGAUGUUUCAGCUC-3' (c7/2), 5'-CCAACUCAAGGUCCAUGCC-3' (c11), 5'-
506 AAACUGGGCUGUACUUUGU-3' (c15/1), 5'- AACUGGGCUGUACUUUGUA-3' (c15/2),
507 5'- CAACAACCUGCCCCUGAGC-3' (c16/1), 5'- AACUCUAAGCGUCCCCAGG-3' (c16/2),
508 5'- UCAACGUAUCUGAGCUCUC-3' (c21), and 5'- AAUCUCAGACGUUUUUCGG-3'
509 (c22).

510 These eight siRNAs were reverse transfected into HeyA8, H460, M565, and 3LL cells using
511 RNAiMAX transfection reagent (ThermoFisher Scientific) at 10 nM in triplicate as previously
512 described (Murmann et al., 2018). The non-targeting (NT) and siL3 siRNAs, as described
513 previously (Putzbach et al., 2017), were used as a negative and positive control, respectively.
514 Cell death was quantified via ATP release 96 hours after transfection using CellTiter-Glo

515 (Promega). The % viability was calculated in relation to the RNAiMAX-only treatment
516 structure (***Figure 4 - figure supplement 1B***).
517
518 **Statistical analyses**
519 Continuous data were summarized as means and standard deviations (except for all IncuCyte
520 experiments where standard errors are shown) and dichotomous data as proportions. Continuous
521 data were compared using t-tests for two independent groups and one-way ANOVA for 3 or
522 more groups. For evaluation of continuous outcomes over time, two-way ANOVA was used with
523 one factor for the treatment conditions of primary interest and a second factor for time treated as
524 a categorical variable to allow for non-linearity.
525 The effects of treatment on wild-type versus Drosha knock-out cells were statistically
526 assessed by fitting regression models that included linear and quadratic terms for value over
527 time, main effects for treatment and cell type, and two- and three-way interactions for treatment,
528 cell-type and time. The three-way interaction on the polynomial terms with treatment and cell
529 type was evaluated for statistical significance since this represents the difference in treatment
530 effects over the course of the experiment for the varying cell types.
531 GSEA used in ***Figure 2B*** was performed using the GSEA v2.2.4 software from the Broad
532 Institute (www.http://software.broadinstitute.org/gsea); 1000 permutations were used. The
533 Sabatini gene lists were set as custom gene sets to determine enrichment of survival genes versus
534 the nonsurvival control genes in downregulated genes from the RNA-Seq data as done
535 previously (Putzbach et al., 2017); p-values below 0.05 were considered significantly enriched.
536 Genes with an average normalized read expression (across both pair of duplicates) below 3 were
537 excluded so as to only include genes that are truly expressed. The GO enrichment analysis shown
538 in ***Figure 2D*** was performed with all genes that after alignment and normalization were found to
539 be at least 1.5 fold downregulated with an adjusted p-value of <0.05 using the software available
540 on www.Metascape.org and default running parameters. The other data sets used in this analysis
541 (HeyA8 cells transfected with a toxic siRNA targeting CD95L siL3 and 293T infected with toxic
542 shRNAs targeting CD95L shL1 and shL3 and HeyA8 cells infected with a toxic shRNA
543 targeting CD95 shR6) were previously described (Putzbach et al., 2017).
544 All statistical analyses were conducted in Stata 14 or R 3.3.1.
545
546 **Data availability**

RNA sequencing data generated for this study is available in the GEO repository: GSE103631 (https://www.ncbi.nlm.nih.gov/geo/query/acc.cgi?acc=GSE103631, reviewer access token: etgbqyaenvirjqn) and GSE114425 (https://www.ncbi.nlm.nih.gov/geo/query/acc.cgi?acc=GSE114425, reviewer access token: edgdoaocjberbyr).

Acknowledgements

We are grateful to Siquan Chen for testing small CD95L-derived siRNAs. M.H. and A.A.S were supported by the Intramural Research Program of NIAMS. A.A.S. acknowledges support by the Swedish Research Council postdoctoral fellowship. This work was funded by training grant T32CA009560 (to W.P. and A.H.K.), R50CA221848 (to E.T.B.), and R35CA197450 (to M.E.P.).

Author contributions

W.P. planned the study and performed experiments. A.H.K., Q.Q.G., A.S.Q., and A.S. performed experiments, D.M.S. provided biostatistics support, E.B. provided biocomputational support, A.A.S. performed the Ago pull down experiments, M.H. provided assistance and discussions on the mechanism of RNAi and the RISC, and M.E.P. directed the study and M.E.P. and W.P. wrote the manuscript.

Competing financial interests

The authors declare no competing financial interests.

570 **Figure legends**
571
572 **Figure 1.**
573 **The CD95L RNA is toxic to cells.**
574 (**A**) *Left*: Schematic of the different CD95L mutants used. *Right:* Percent cell confluence over
575 time of HeyA8 parental cells in the absence (*left panel*) or in the presence of 20 μM zVAD-fmk
576 (*center panel*), or CD95 k.o. cells (*right panel*) after expression of CD95L constructs. Data are
577 representative of one to three independent experiments. Values were calculated from samples
578 done in triplicate or quadruplicate shown as mean ± SE. (**B**) *Left*: Western blot analysis of
579 HeyA8 cells overexpressing different CD95L mutant RNAs. Cells expressing $CD95L^{MUT}$ or
580 CD95L were pretreated with 20 μM zVAD-fmk. Note the small amount of truncated CD95L in
581 cells infected with CD95L MUT-NP does not have CD95 binding activity. Very similar data
582 were obtained when the constructs were expressed in either CD95 k.o. HeyA8 cells (clone #11)
583 or NB 7 cells, both without treatment with zVAD (data not shown). *Right*: RT-qPCR analysis for
584 CD95L of the same samples. Data are representative of two independent experiments. Each bar
585 represents mean ± S.D. of three replicates. (**C**, **D**) Quantification of cell death (**C**) and ROS
586 production (**D**) in cells expressing either pLenti (v) or pLenti-CD95L (L) at different time points
587 (days after infection). Data are representative of two independent experiments. Each bar
588 represents mean ± SE of three replicates. * $p<0.05$, ** $p<0.001$, *** $p<0.0001$, unpaired t-test.
589 (**E**) Confluency over time of the MCF-7 complete CD95 k.o. FA4 clone (right) or a MCF-7 clone
590 #21 in which we deleted the shR6 site resulting in an out-of-frame shift after infection with either
591 vector control or wt CD95L. Data are representative of two independent experiments. Each data
592 point represents mean ± SE of three replicates.
593
594 **Figure 1 - figure supplement 1.**
595 **Generation of complete CD95 k.o. MCF-7 cells.**
596 (**A**) Schematic of the genomic locations and sequences of the gRNAs used to excise the entire
597 CD95 gene in MCF-7 cells. PAM site is underlined. (**B**) PCR with flanking (*top panels*) and
598 internal (*bottom panels*) primers used to confirm the absence of the CD95 gene in MCF-7 clones.
599 Parental (Par.) cells and three clones infected with Cas9 only (Cas9) and two complete k.o.
600 clones (F2 and FA4) are shown. (**C**) RT-qPCR analysis of the indicated clones using primers
601 spanning either exon 1/2 or exon 2/3 of the CD95 gene. (**D**) Surface staining for CD95 of one wt
602 and one k.o. clone. (**E**) Western blot analysis of all clones.
603
604 **Figure 1 - figure supplement 2.**
605 **Toxicity of CD95L mRNA is independent of CD95L protein expression.**
606 (**A**) Schematic showing the positions of the silent mutation of the $CD95L^{SIL}$ compared to wild
607 type CD95L. (**B**) Percent cell confluence over time of HeyA8 CD95 k.o. cells over-expressing
608 empty pLenti, wild-type CD95L (from two separately cloned viruses), or the $CD95L^{SIL}$. (**C**) RT-
609 qPCR analysis and Western blot (*inset*) of wild type CD95L and $CD95L^{SIL}$ mutant mRNAs in the
610 over-expressing cells shown in **B**.
611
612 **Figure 2.**
613 **Toxicity induced by CD95L overexpression is reminiscent of DISE.**
614 (**A**) Phase-contrast images of HeyA8 and HeyA8 CD95 k.o. cells after infection with pLKO-
615 shScr/shL3 or pLenti/pLenti-CD95L, respectively, at the indicated time point. (**B**) Gene set
616 enrichment analysis for the 1846 survival genes (*top panel*) and the 416 nonsurvival genes
617 (*bottom panel*) identified in the Sabatini study (Putzbach et al., 2017; Wang et al., 2015) of

mRNAs downregulated in CD95L expressing HeyA8 CD95 k.o. cells compared to HeyA8 CD95 k.o. cells infected with pLenti virus. p-values indicate the significance of enrichment. (**C**) The genes downregulated in all cells including the ones downregulated following introduction of one of four si/shRNAs (Putzbach et al., 2017) derived from either CD95 or CD95L (see ***Figure 2D***) and the ones overexpressing CD95L ORF as described in **B**. (**D**) Metascape analysis of 5 RNA Seq data sets analyzed. The boxed GO term clusters were highly enriched in all 5 data sets.

Figure 3.

Small RNAs generated in cells expressing CD95L mRNA are loaded into the RISC.

(**A**) Percent cell confluence over time of HCT116 parental (*left*) or Drosha k.o. (*right*) cells after infection with CD95^{MUT}NP. Data are representative of three independent experiments. Each data point represents the mean ± SE of three replicates. *Inset:* Phase contrast images of Drosha k.o. cells 9 days after infection with either empty vector or CD95L^{MUT}NP. (**B**) Percent cell confluence of HeyA8 CD95 k.o. cells transfected with either non-targeting siRNA (siCtr) or a pool of 4 siRNAs targeting AGO2 following subsequent infection with either empty pLenti (EV) or pLenti CD95L. *Inset:* Western blot showing successful knock-down of human AGO2. (**C**) *Top*: autoradiograph on RNAs pulled down with the Ago binding peptide. *Bottom*: Western blot analysis of pulled down Ago proteins. v, pLenti; L, pLenti-CD95L expressing cells. (**D**) Pie charts showing the relative ratio of small RNAs pulled down with the Ago proteins in wt and Drosha k.o. cells. Depicted are all the amounts of all small RNAs that contributed at least 0.01% to the total RNA content. Only in the Drosha k.o. cells was a significant amount of CD95L derived Ago bound reads found. They represented the 75th most abundant small RNA species (arrow). The average number of total sequenced reads (of two duplicates) are shown for each condition. (**E**) *Top*: Number of reads (normalized per million) of the top six most abundant small RNAs in the RISC of either HCT116 wt-pLenti or -pLenti-CD95L cells. *Bottom*: Number of reads (per million) of the top five genes with small RNAs most abundant in the RISC of either HCT116 Drosha k.o. pLenti, or -pLenti-CD95L cells and of CD95L derived. Note: miR-21 is not included as it is already shown in the top row. Bottom right panel: Abundance of Ago bound CD95L derived small RNAs. Shown in all panels is the abundance of RNAs in the four samples. Rep 1 and rep 2, replicate 1 and 2.

Figure 4

The entire CD95L mRNA gives rise to small RNAs that bind to the RISC.

(**A**) Length distribution of CD95L derived reads in various analyses. (**B, C**) Read alignment with CD95L^{MUT}NP ORF of analyses of small RNAs pulled down with Ago proteins from HCT116 wt (**B**, top) and Drosha k.o. (**B**, bottom) cells and of total small RNAs from HCT116 Drosha k.o. cells (**C**) after infection with CD95L^{MUT}NP. (**D, E**) Read alignment with wt CD95L ORF of analyses of small RNAs pulled down with Ago proteins (**D**) or total small RNAs (**E**) from HeyA8 CD95 k.o. cells after infection with wt CD95L. (**F**) Percent cell confluence over time of HCT116 parental (*top*) or Dicer k.o. (clone #43) (*bottom*) cells after infection with CD95^{MUT}NP. (Dicer k.o. clone #45, gave a similar result, data not shown). Data are representative of two independent experiments. Each data point represents the mean ± SE of three replicates. (**G**) RT-qPCR analysis of clusters 8 and 21 in HCT116 parental, Dicer k.o. (clone #43), and Drosha k.o. cells after infection with CD95^{MUT}NP. Each bar represents mean ± S.D. of three replicates. v, vector, L, CD95L expressing cells.

Figure 4 - figure supplement 1

Predicted secondary structure of CD95L ORF and toxicity of CD95L-derived small RNAs after conversion to siRNAs.

(**A**) The $CD95L^{MUT}NP$ RNA was subjected to a RNA secondary structure analysis (http://rna.tbi.univie.ac.at) using default settings. The locations of 22 reads representative of the 22 read clusters are shown. Regions with potential duplex formation are boxed. The oligonucleotides that were found to be toxic when expressed as siRNAs are circled. (**B**) Toxicity of the eight siRNAs designed using the CD95L-derived small RNA fragments bound to Ago as the antisense strand sequences 96 hours post-transfection in the indicated cell lines. Each data point represents the mean ± SE of three replicates.

Supplementary Videos:

Video 1: CD95 k.o. HeyA8 cells (clone 11) infected with pLenti control virus.

Video 2: CD95 k.o. HeyA8 cells (clone 11) infected with pLenti-CD95Lvirus.

Video 3: HeyA8 cells infected with pLKO-shScr.

Video 4: HeyA8 cells infected with pLKO-shL3.

687 **References**
688

689 Algeciras-Schimnich, A., Shen, L., Barnhart, B. C., Murmann, A. E., Burkhardt, J. K., & Peter,
690 M. E. (2002). Molecular ordering of the initial signaling events of CD95. *Mol Cell Biol,*
691 *22*(1), 207-220.
692 Ceppi, P., Hadji, A., Kohlhapp, F., Pattanayak, A., Hau, A., Xia, L., . . . Peter, M. E. (2014).
693 CD95 and CD95L promote and protect cancer stem cells. *Nature Commun, 5*, 5238.
694 Elkayam, E., Faehnle, C. R., Morales, M., Sun, J., Li, H., & Joshua-Tor, L. (2017). Multivalent
695 Recruitment of Human Argonaute by GW182. *Mol Cell, 67*(4), 646-658 e643.
696 doi:10.1016/j.molcel.2017.07.007
697 ElOjeimy, S., McKillop, J. C., El-Zawahry, A. M., Holman, D. H., Liu, X., Schwartz, D. A., . . .
698 Norris, J. S. (2006). FasL gene therapy: a new therapeutic modality for head and neck
699 cancer. *Cancer gene therapy, 13*(8), 739-745. doi:10.1038/sj.cgt.7700951
700 Friesen, C., Fulda, S., & Debatin, K. M. (1999). Cytotoxic drugs and the CD95 pathway.
701 *Leukemia, 13*(11), 1854-1858.
702 Fu, Q., Fu, T. M., Cruz, A. C., Sengupta, P., Thomas, S. K., Wang, S., . . . Chou, J. J. (2016).
703 Structural Basis and Functional Role of Intramembrane Trimerization of the Fas/CD95
704 Death Receptor. *Mol Cell, 61*(4), 602-613. doi:10.1016/j.molcel.2016.01.009
705 Gao, Q. Q., Putzbach, W., Murmann, A. E., Chen, S., Ambrosini, G., Peter, J. M., . . . Peter, M.
706 E. (2018). 6mer Seed Toxicity Determines Strand Selection in miRNAs. *BioRxive*.
707 doi:https://doi.org/10.1101/284406
708 Hadji, A., Ceppi, P., Murmann, A. E., Brockway, S., Pattanayak, A., Bhinder, B., . . . Peter, M.
709 E. (2014). Death induced by CD95 or CD95 ligand elimination. *Cell Reports, 10*, 208-
710 222.
711 Hafner, M., Renwick, N., Farazi, T. A., Mihailovic, A., Pena, J. T., & Tuschl, T. (2012).
712 Barcoded cDNA library preparation for small RNA profiling by next-generation
713 sequencing. *Methods, 58*(2), 164-170. doi:10.1016/j.ymeth.2012.07.030
714 Hamilton, A. J., & Baulcombe, D. C. (1999). A species of small antisense RNA in
715 posttranscriptional gene silencing in plants. *Science, 286*(5441), 950-952.
716 Hansen, T. B., Veno, M. T., Jensen, T. I., Schaefer, A., Damgaard, C. K., & Kjems, J. (2016).
717 Argonaute-associated short introns are a novel class of gene regulators. *Nature*
718 *communications, 7*, 11538. doi:10.1038/ncomms11538
719 Hauptmann, J., Schraivogel, D., Bruckmann, A., Manickavel, S., Jakob, L., Eichner, N., . . .
720 Meister, G. (2015). Biochemical isolation of Argonaute protein complexes by Ago-APP.
721 *Proc Natl Acad Sci U S A, 112*(38), 11841-11845. doi:10.1073/pnas.1506116112
722 Hyer, M. L., Voelkel-Johnson, C., Rubinchik, S., Dong, J., & Norris, J. S. (2000). Intracellular
723 Fas ligand expression causes Fas-mediated apoptosis in human prostate cancer cells
724 resistant to monoclonal antibody-induced apoptosis. *Mol Ther, 2*(4), 348-358.
725 Kim, Y. K., Kim, B., & Kim, V. N. (2016). Re-evaluation of the roles of DROSHA, Export in 5,
726 and DICER in microRNA biogenesis. *Proc Natl Acad Sci U S A, 113*(13), E1881-1889.
727 doi:10.1073/pnas.1602532113
728 Liu, J., Carmell, M. A., Rivas, F. V., Marsden, C. G., Thomson, J. M., Song, J. J., . . . Hannon,
729 G. J. (2004). Argonaute2 is the catalytic engine of mammalian RNAi. *Science,*
730 *305*(5689), 1437-1441.
731 Mali, P., Yang, L., Esvelt, K. M., Aach, J., Guell, M., DiCarlo, J. E., . . . Church, G. M. (2013).
732 RNA-guided human genome engineering via Cas9. *Science, 339*(6121), 823-826.
733 doi:10.1126/science.1232033

Murmann, A. E., Gao, Q. Q., Putzbach, W. E., Patel, M., Bartom, E. T., Law, C. Y., . . . Peter, M. E. (2018). Small interfering RNAs based on huntingtin trinucleotide repeats are highly toxic to cancer cells. *EMBO Rep, 19*(3). doi:10.15252/embr.201745336

Nisihara, T., Ushio, Y., Higuchi, H., Kayagaki, N., Yamaguchi, N., Soejima, K., . . . Yagita, H. (2001). Humanization and epitope mapping of neutralizing anti-human Fas ligand monoclonal antibodies: structural insights into Fas/Fas ligand interaction. *J Immunol, 167*(6), 3266-3275.

Patel, M., & Peter, M. E. (2017). Identification of DISE-inducing shRNAs by monitoring cellular responses. *Cell Cycle*, 0. doi:10.1080/15384101.2017.1383576

Putzbach, W., Gao, Q. Q., Patel, M., Haluck-Kangas, A., Murmann, A. E., & Peter, M. E. (2018). DISE - A Seed Dependent RNAi Off-Target Effect that Kills Cancer Cells. *Trends in Cancer, 4*, 10-19.

Putzbach, W., Gao, Q. Q., Patel, M., van Dongen, S., Haluck-Kangas, A., Sarshad, A. A., . . . Peter, M. E. (2017). Many si/shRNAs can kill cancer cells by targeting multiple survival genes through an off-target mechanism. *Elife, 6*, e29702.

Robinson, M. D., McCarthy, D. J., & Smyth, G. K. (2010). edgeR: a Bioconductor package for differential expression analysis of digital gene expression data. *Bioinformatics, 26*(1), 139-140. doi:10.1093/bioinformatics/btp616

Schneider, P., Bodmer, J. L., Holler, N., Mattmann, C., Scuderi, P., Terskikh, A., . . . Tschopp, J. (1997). Characterization of Fas (Apo-1, CD95)-Fas ligand interaction. *J Biol Chem, 272*(30), 18827-18833.

Suda, T., Takahashi, T., Golstein, P., & Nagata, S. (1993). Molecular cloning and expression of the Fas ligand, a novel member of the tumor necrosis factor family. *Cell, 75*(6), 1169-1178.

Sudarshan, S., Holman, D. H., Hyer, M. L., Voelkel-Johnson, C., Dong, J. Y., & Norris, J. S. (2005). In vitro efficacy of Fas ligand gene therapy for the treatment of bladder cancer. *Cancer gene therapy, 12*(1), 12-18. doi:10.1038/sj.cgt.7700746

Sun, H., Liu, Y., Bu, D., Liu, X., Norris, J. S., & Xiao, S. (2012). Efficient growth suppression and apoptosis in human laryngeal carcinoma cell line HEP-2 induced by an adeno-associated virus expressing human FAS ligand. *Head Neck, 34*(11), 1628-1633. doi:10.1002/hed.21985

Wang, T., Birsoy, K., Hughes, N. W., Krupczak, K. M., Post, Y., Wei, J. J., . . . Sabatini, D. M. (2015). Identification and characterization of essential genes in the human genome. *Science, 350*(6264), 1096-1101. doi:10.1126/science.aac7041

Yoda, M., Cifuentes, D., Izumi, N., Sakaguchi, Y., Suzuki, T., Giraldez, A. J., & Tomari, Y. (2013). Poly(A)-specific ribonuclease mediates 3'-end trimming of Argonaute2-cleaved precursor microRNAs. *Cell Rep, 5*(3), 715-726. doi:10.1016/j.celrep.2013.09.029

Figure 1

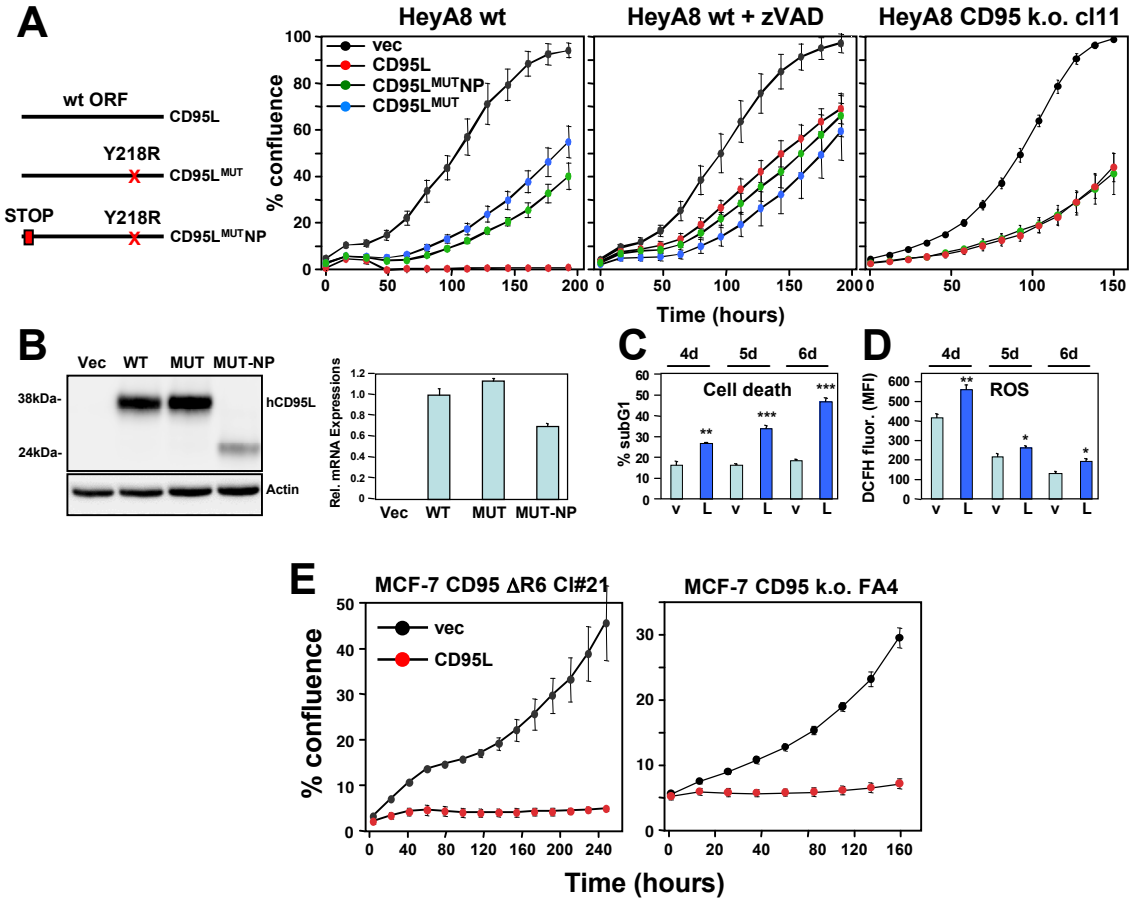
A
wt ORF
CD95L
Y218R
CD95L^MUT
STOP
Y218R
CD95L^MUTNP
HeyA8 wt
HeyA8 wt + zVAD
HeyA8 CD95 k.o. cl11
vec
CD95L
CD95L^MUTNP
CD95L^MUT
% confluence
Time (hours)
B
Vec WT MUT MUT-NP
38kDa-
24kDa-
hCD95L
Actin
Rel. mRNA Expressions
Vec WT MUT MUT-NP
C
4d 5d 6d
Cell death
% subG1
v L v L v L
D
4d 5d 6d
ROS
DCFH fluor. (MFI)
v L v L v L
E
MCF-7 CD95 ΔR6 Cl#21
MCF-7 CD95 k.o. FA4
vec
CD95L
% confluence
Time (hours)

Figure 1 - figure supplement 1

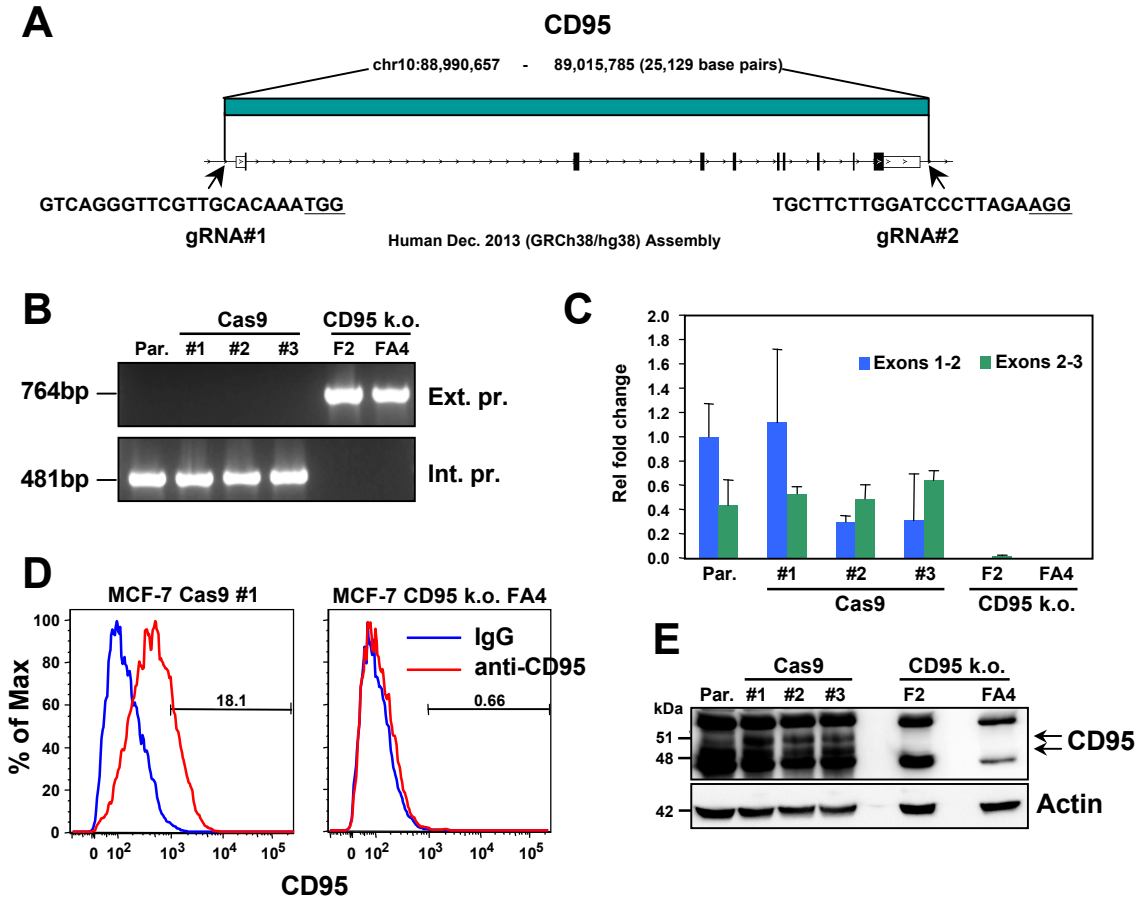

Figure 1 - figure supplement 2

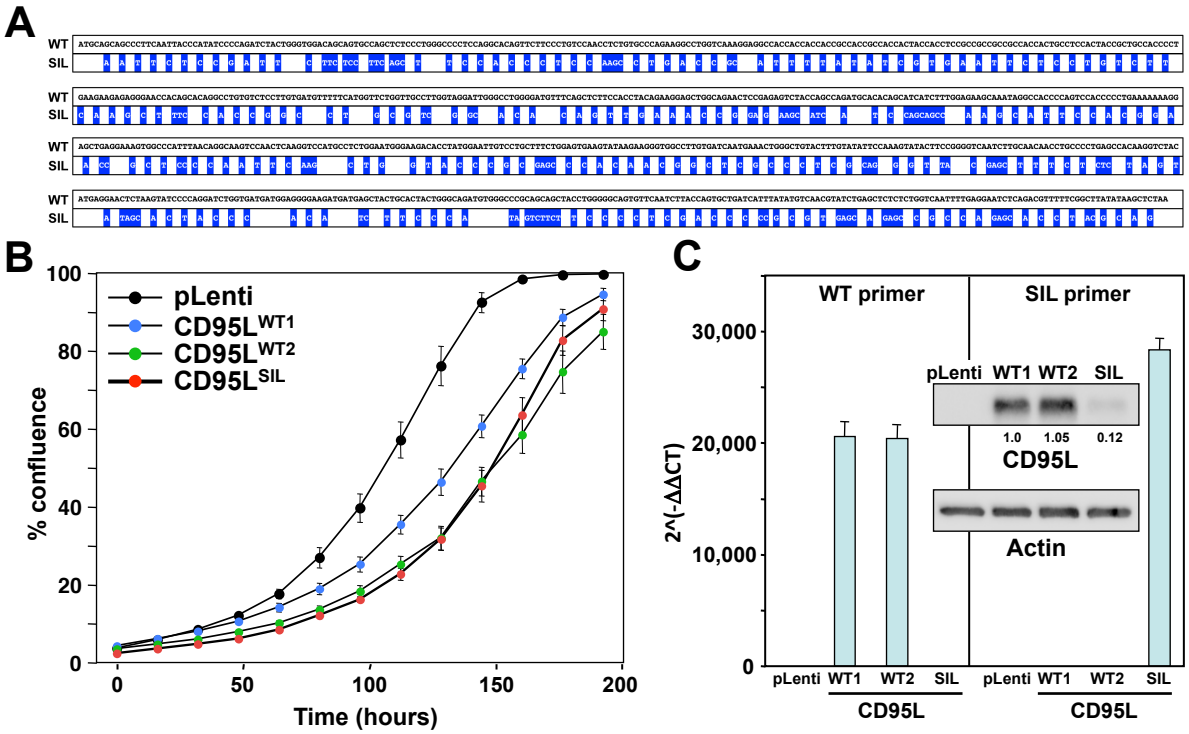

Figure 2

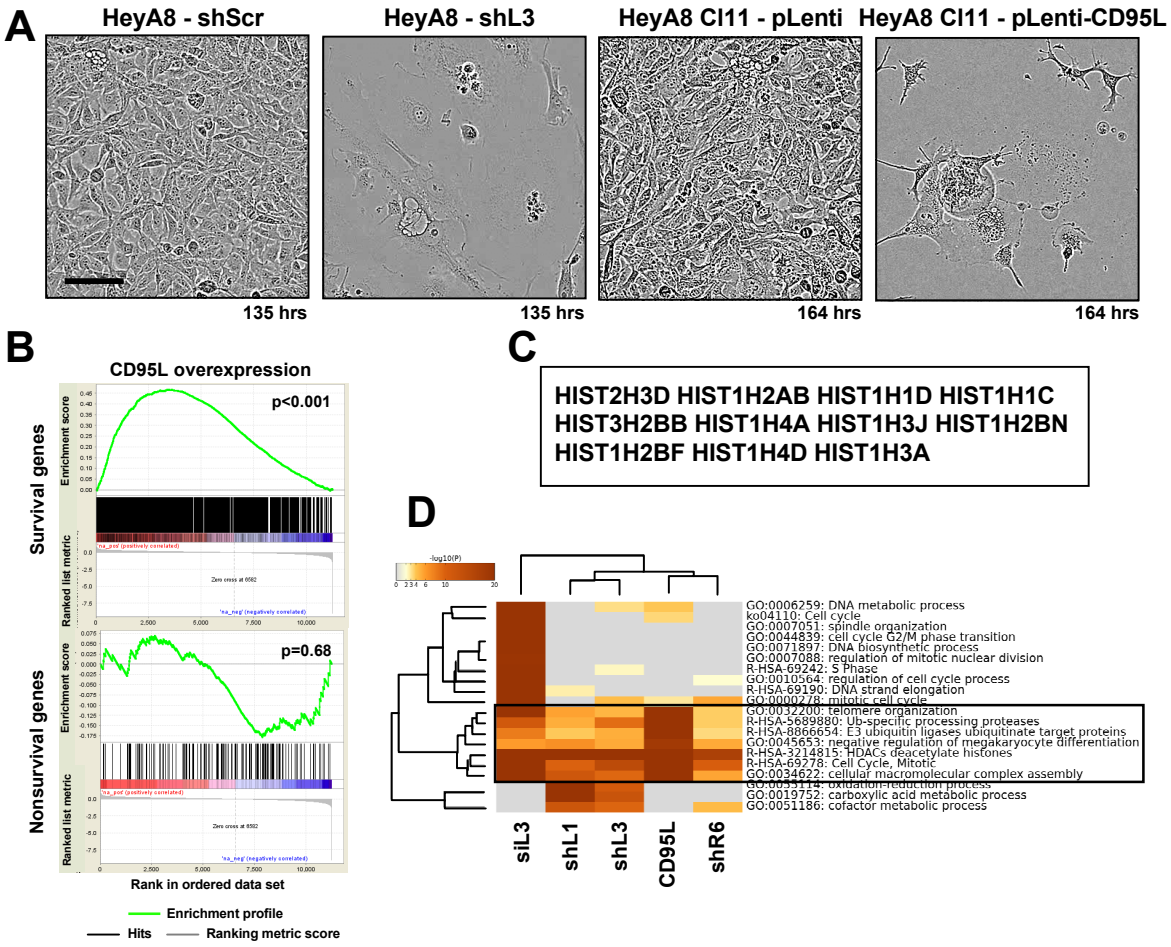
A
HeyA8 - shScr
HeyA8 - shL3
HeyA8 Cl11 - pLenti
HeyA8 Cl11 - pLenti-CD95L
135 hrs
135 hrs
164 hrs
164 hrs
B
CD95L overexpression
Survival genes
Nonsurvival genes
p<0.001
p=0.68
Enrichment score
Ranked list metric
Rank in ordered data set
Enrichment profile
Hits
Ranking metric score
C
HIST2H3D HIST1H2AB HIST1H1D HIST1H1C
HIST3H2BB HIST1H4A HIST1H3J HIST1H2BN
HIST1H2BF HIST1H4D HIST1H3A
D
-log10(P)
GO:0006259: DNA metabolic process
ko04110: Cell cycle
GO:0007051: spindle organization
GO:0044839: cell cycle G2/M phase transition
GO:0071897: DNA biosynthetic process
GO:0007088: regulation of mitotic nuclear division
R-HSA-69242: S Phase
GO:0010564: regulation of cell cycle process
R-HSA-69190: DNA strand elongation
GO:0000278: mitotic cell cycle
GO:0032200: telomere organization
R-HSA-5689880: Ub-specific processing proteases
R-HSA-8866654: E3 ubiquitin ligases ubiquitinate target proteins
GO:0045653: negative regulation of megakaryocyte differentiation
R-HSA-3214815: HDACs deacetylate histones
R-HSA-69278: Cell Cycle, Mitotic
GO:0034622: cellular macromolecular complex assembly
GO:0055114: oxidation-reduction process
GO:0019752: carboxylic acid metabolic process
GO:0051186: cofactor metabolic process
siL3
shL1
shL3
CD95L
shR6

Figure 3

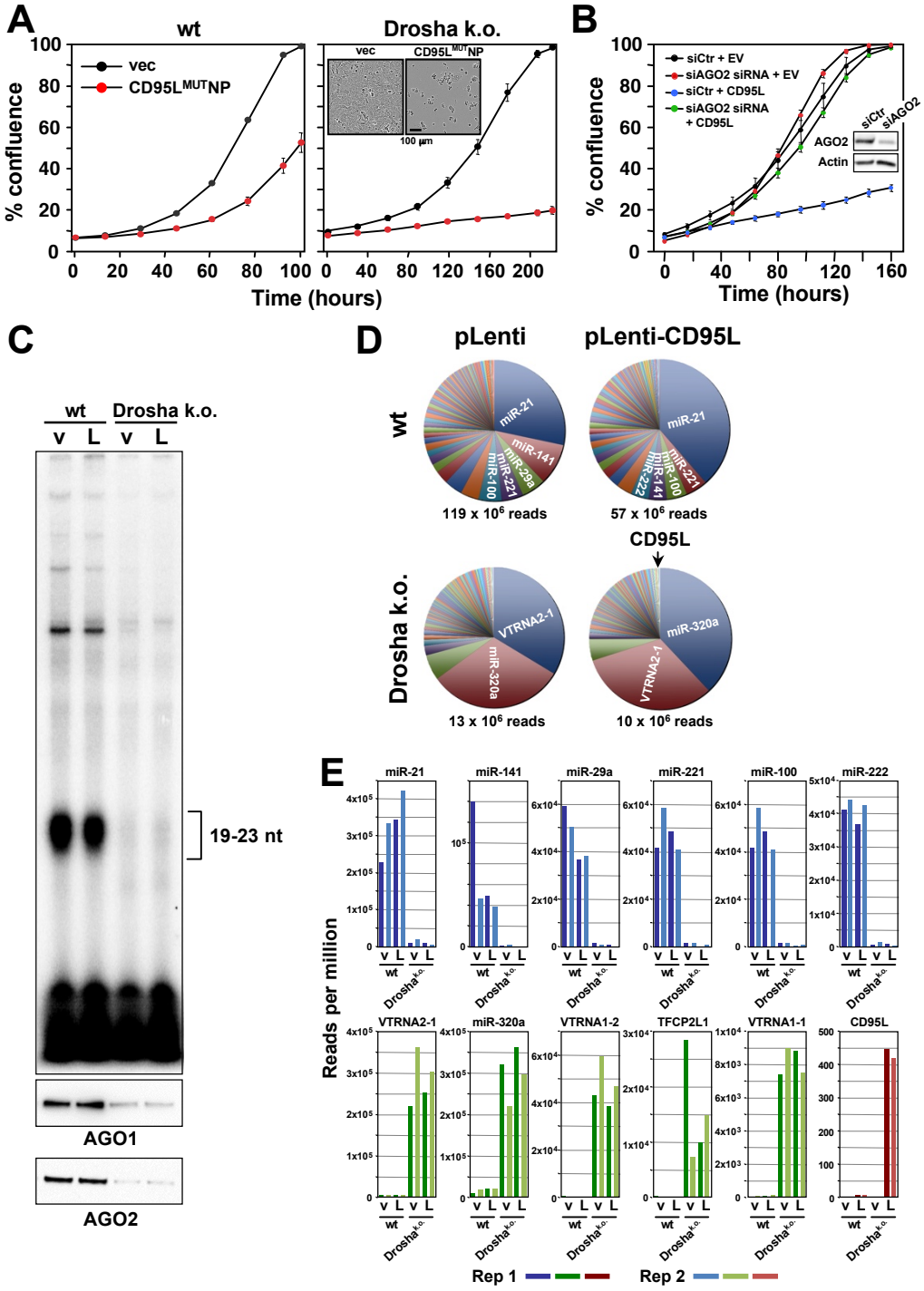
A
wt
Drosha k.o.
vec
CD95L^MUT NP
100 µm
% confluence
Time (hours)
B
siCtr + EV
siAGO2 siRNA + EV
siCtr + CD95L
siAGO2 siRNA + CD95L
siCtr
siAGO2
AGO2
Actin
C
wt
Drosha k.o.
v L v L
19-23 nt
AGO1
AGO2
D
pLenti
pLenti-CD95L
wt
Drosha k.o.
miR-21
miR-141
miR-29a
miR-221
miR-100
miR-222
119 x 10^6 reads
57 x 10^6 reads
CD95L
VTRNA2-1
miR-320a
13 x 10^6 reads
10 x 10^6 reads
E
Reads per million
miR-21
miR-141
miR-29a
miR-221
miR-100
miR-222
VTRNA2-1
miR-320a
VTRNA1-2
TFCP2L1
VTRNA1-1
CD95L
Rep 1
Rep 2

Figure 4

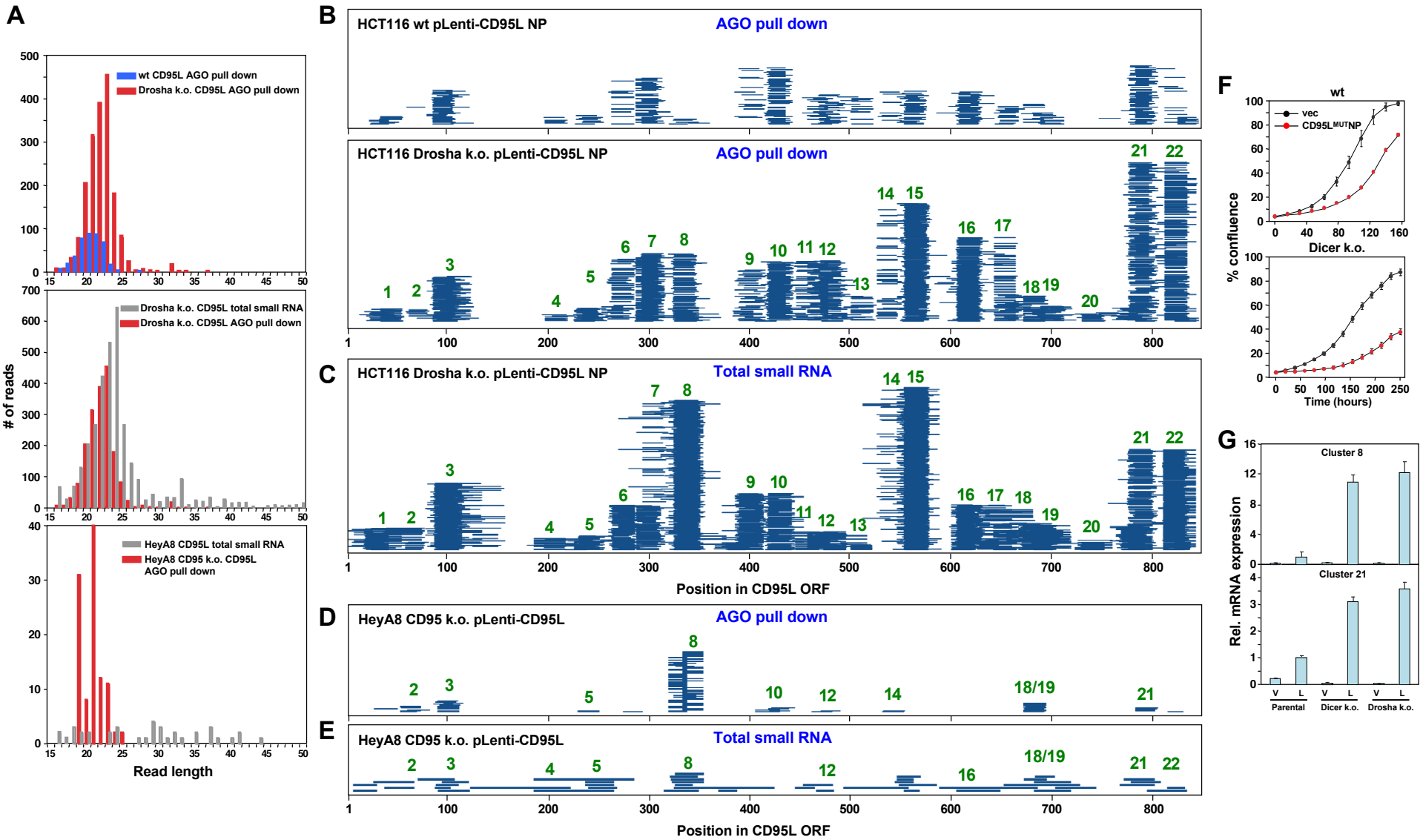
A
wt CD95L AGO pull down
Drosha k.o. CD95L AGO pull down
Drosha k.o. CD95L total small RNA
Drosha k.o. CD95L AGO pull down
HeyA8 CD95L total small RNA
HeyA8 CD95 k.o. CD95L AGO pull down
# of reads
Read length
B
HCT116 wt pLenti-CD95L NP
AGO pull down
HCT116 Drosha k.o. pLenti-CD95L NP
AGO pull down
C
HCT116 Drosha k.o. pLenti-CD95L NP
Total small RNA
Position in CD95L ORF
D
HeyA8 CD95 k.o. pLenti-CD95L
AGO pull down
E
HeyA8 CD95 k.o. pLenti-CD95L
Total small RNA
Position in CD95L ORF
F
wt
vec
CD95L MUT NP
Dicer k.o.
% confluence
Time (hours)
G
Cluster 8
Cluster 21
Rel. mRNA expression
V
L
Parental
Dicer k.o.
Drosha k.o.
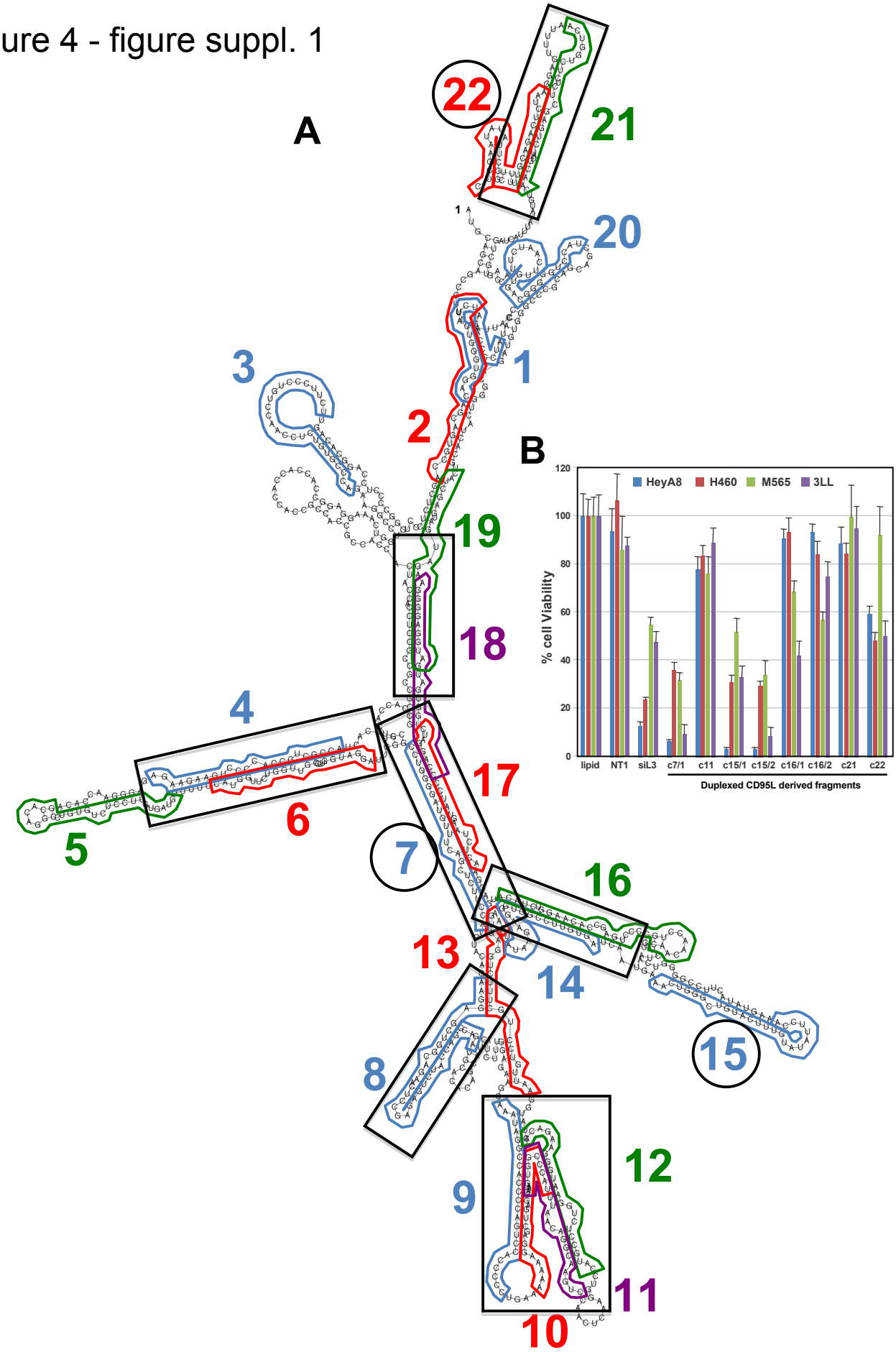
Figure 4 - figure suppl. 1